

1
2
3
4
5
6
7
8
9

a Coriolis tutorial, Part 2:

a rotating shallow water model, potential vorticity balance and geostrophic adjustment

James F. Price
Woods Hole Oceanographic Institution
Woods Hole, Massachusetts, 02543
www.whoi.edu/science/PO/people/jprice jprice@whoi.edu

Version 8 October 15, 2018

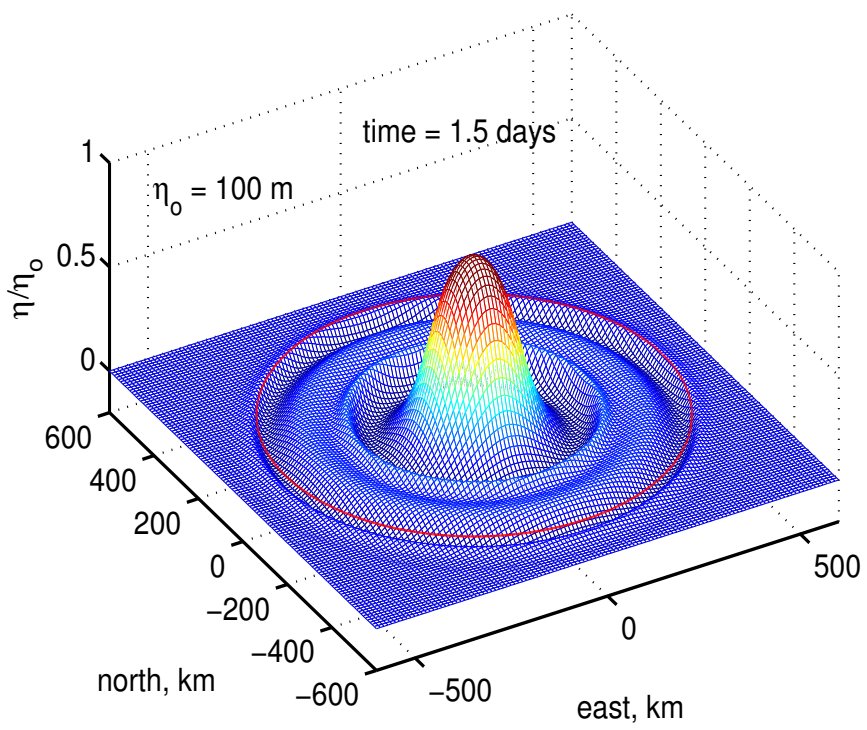


Figure 1: A snapshot taken 1.5 days after the start of a numerical experiment on geostrophic adjustment: a thickness anomaly of a dense fluid was released from rest onto an f -plane centered on 30°N and allowed to evolve freely under the effects of gravity and rotation. The thickness anomaly slumps noticeably within the first half day, which excites inertia-gravity waves that expand isotropically. The leading edge propagates at the rate of a long, non-dispersive baroclinic gravity wave, roughly 275 km day^{-1} in this case. After about ten days the inertia-gravity wave radiation was largely completed, leaving most of the height anomaly seen here in a near geostrophic balance. An animation of this experiment is online at www.whoi.edu/jpweb/ga2d-h100-f.mp4

10 **Abstract:** This is the second of a four-part introduction to the effects of Earth’s rotation on the fluid
 11 dynamics of the atmosphere and ocean. Part 1 derived the Coriolis force, $\propto -f\mathbf{k}\times\mathbf{V}$, where f is the
 12 Coriolis parameter, \mathbf{k} is the vertical unit vector, and \mathbf{V} is horizontal wind or current, and went on to
 13 analyze some of its basic properties in the context of a very simple, single parcel model. The goal and
 14 plan of this Part 2 is to develop further insight into the consequences of the Coriolis force by analyzing
 15 a sequence of experiments in which a thickness anomaly of horizontal scale L is released from rest and
 16 allowed to evolve under the influence of gravity and the Coriolis force. These geostrophic adjustment
 17 experiments are posed in a single layer fluid model, often called the shallow water model.

18 The initial gravitational slumping produces gravity waves (see the cover graphic). If there is no
 19 rotation, i.e., if $f = 0$, gravity waves will disperse the mass anomaly in a time L/C , where C is the
 20 gravity wave phase speed. When rotation is present, and if L exceeds several times the radius of
 21 deformation, $R_d = C/f$, and assuming that the eddy has a potential vorticity anomaly, then the Coriolis
 22 force will arrest the gravitational slumping and yield a geostrophically balanced eddy, an anti-cyclone if
 23 the thickness anomaly was a mass excess (high pressure). If f is constant and if there is no friction, then
 24 a geostrophically balanced eddy could be exactly steady. If the eddy is small horizontally and intense in
 25 the sense that the Rossby number is appreciable, say $U/fL \geq 0.1$, where U is the current, then
 26 curvature will modify the geostrophic balance.

27 These and other low frequency phenomenon are often best interpreted in the context of potential
 28 vorticity conservation, the geophysical fluid equivalent of angular momentum conservation. Earth’s
 29 rotation contributes planetary vorticity $= f$, that is generally considerably larger than the relative
 30 vorticity of winds and currents. Small changes in the thickness of a fluid column will cause significant
 31 changes in the relative vorticity of winds and currents.

32 Contents

33	1 Large-scale flows of the atmosphere and ocean	4
34	2 Shallow water model	7
35	2.1 Mass and momentum balance of an ideal fluid layer	9
36	2.2 Solving and diagnosing the shallow water system	14
37	2.2.1 Wave velocities and fluid velocities	14
38	2.2.2 Energy balance	16
39	2.2.3 Potential vorticity balance	17
40	2.2.4 Linear and nonlinear; finite amplitude effects	22

41	2.3	Boundary and initial conditions define the problem	23
42	2.4	Appendix to Sec. 2: Normal modes of a two layer model ocean	24
43	2.4.1	Barotropic normal mode	27
44	2.4.2	Baroclinic normal mode	30
45	2.4.3	Reduced gravity approximation of the baroclinic normal mode	31
46	2.5	Problems	31
47	3	Gravitational adjustment	34
48	3.1	Just gravity waves	34
49	3.2	An exact solution of the linear, one-dimensional wave equation	36
50	3.3	The choice of scales	37
51	3.4	Energy and potential vorticity balances	38
52	3.5	Finer details of the solution; finite amplitude effects	39
53	3.6	Problems	41
54	4	Geostrophic adjustment on an f-plane	42
55	4.1	Dispersion relation for waves on an f -plane	42
56	4.2	Intrinsic scales of the f -plane	45
57	4.3	Gravity, inertial and geostrophic motions	46
58	4.4	The steady state inferred from potential vorticity conservation	49
59	4.5	If there is no potential vorticity anomaly	53
60	4.6	Problems	54
61	5	In two dimensions	54
62	5.1	Adjustment	55
63	5.2	Curvature and Rossby number	55
64	5.3	Problems	60
65	6	Closing remarks	61
66	6.1	Summary	61
67	6.2	What comes next?	63
68	6.3	Supplementary material	63
69		Index	65

1 Large-scale flows of the atmosphere and ocean

This essay is the second of a four-part introduction to fluid dynamics on a rotating Earth. It is written for students who have some preparation in classical dynamics and applied mathematics and who are beginning a quantitative study of geophysical fluid dynamics. Part 1 examined the origin and fundamental properties of the Coriolis force, and went on to consider a few of its consequences in the context of a single parcel model. The Coriolis force, often called simply 'rotation', admits two new modes of motion, a free oscillation usually called an inertial oscillation, and if there is a steady or time-mean forcing, a steady or time-mean motion that is an analogue of geostrophic motion in the atmosphere and ocean.

The broad goal of this Part 2 is to develop further insight into the consequences of rotation in the context of a fluid model, called the shallow water model, derived in Sec. 2. The specific goal is to understand: **What circumstances lead to quasi-steady, nearly geostrophic balance?** We noted in Part 1 that geostrophy was characteristic of most large scale extra-tropical circulation, and now the goal is to flesh out what we mean by 'large scale'. The plan is to solve and analyze a sequence of geostrophic adjustment experiments in which a mass anomaly is released into a rotating environment and allowed to evolve freely under the influence of gravity and rotation. As we will see first in Sec. 3.2, a nearly steady, nearly geostrophic state will follow spontaneously when a mass anomaly is released from rest (zero initial current) provided that the mass anomaly has a sufficiently large horizontal scale, about 100 kilometers or greater at mid-latitudes. On the other hand, mass anomalies having a smaller horizontal scale, or an initial current field that is characteristic of a gravity wave, will be more or less dispersed into gravity waves before reaching a geostrophic balance.

The discussion of the geostrophic adjustment experiments coming next will be based largely upon four noteworthy topics and themes that you will encounter again and again in your study of the atmosphere and ocean:

Wave Dynamics As previewed in the cover graphic, most of the phenomena that arise in these experiments are wave-like. There are gravity waves that are more or less modified by rotation depending upon their wavelength and f , and nearly geostrophic eddies¹ that may also exhibit wave-like propagation (when the β -effect is included in Part 3). The language and concepts appropriate to waves — dispersion relations, phase speed, group speed — are thus essential for the description of the phenomena that arise in the these experiments.

Potential Vorticity Balance The dynamics of low frequency, quasi-geostrophic atmospheric and

¹The term 'eddy' is widely used in fluid dynamics, and with a wide range of meanings. Here eddy means a flow feature having a more or less circular planform, but with no particular dynamics or time-dependence implied. To say that a movement is 'propagation' is suggestive of wave propagation, which is intended.

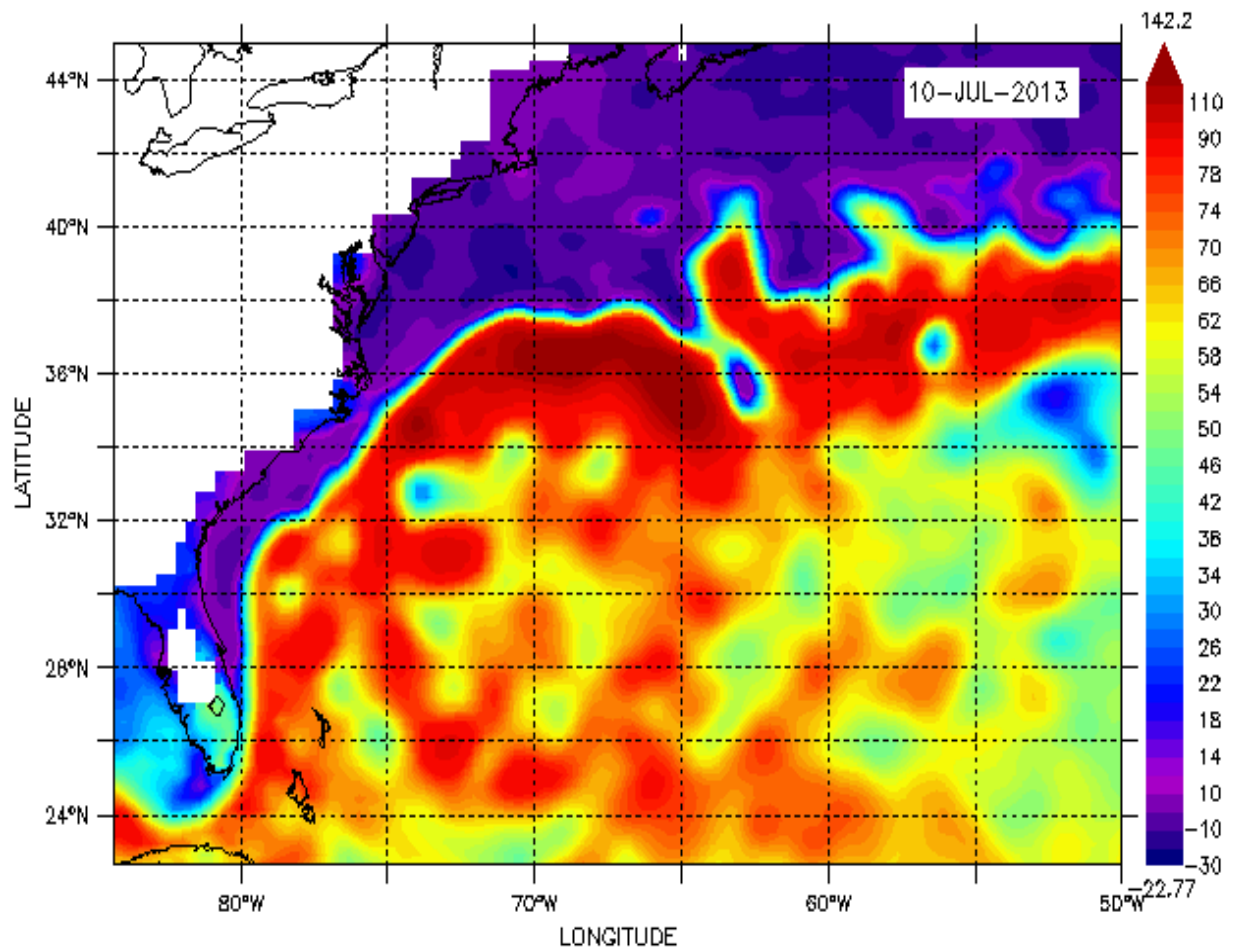


Figure 2: A snapshot of sea surface height, SSH, over the North Atlantic ocean from July, 2013 (thanks to the Aviso project). Compared with the year-long mean of Fig. (1), Part 1, this field shows considerable variability on scales of several hundred kilometers, often termed the oceanic mesoscale (*meso* is Greek for middle) especially in subtropical and higher latitudes. Mesoscale eddies persist as identifiable features for many weeks and have an amplitude of about ± 0.1 m. The corresponding thermocline displacements are about ± 50 m (not evident in this figure). The specific goal of this essay is to understand how Earth's rotation leads to long-lived eddies and gyres that are in approximate geostrophic balance.

101 oceanic phenomena is revealed most effectively by analyzing the balance of potential vorticity,
102 essentially the angular momentum of a rotating fluid, Sec. 2.3.2, rather than by the balance of linear
103 momentum, which was all that was possible for the point-like parcel of Part 1. This use of potential
104 vorticity balance was introduced by Rossby and colleagues in the 1930s² and remains an invaluable tool
105 for the analysis and prediction of large scale and low frequency geophysical flows. Potential vorticity
106 balance will be a central theme here and in Part 3.

107 **Linear and Nonlinear, Finite Amplitude** Waves that arise in linear systems, or in the limit that
108 amplitude goes to zero in the solution of a nonlinear system, will have the most accessible description,
109 e.g., dispersion relation. On the other hand, many geophysical phenomenon have an amplitude large
110 enough that linear dynamics will not be strictly valid. Nevertheless, linear theory will generally be the
111 starting point for an analyses that may then include finite amplitude effects in more comprehensive
112 (numerical) solution methods.

113 **Numerical Models and Solutions** The shallow water system used here is kept as simple as possible
114 but is nevertheless nonlinear, as are all more or less complete fluid models. Solving this nonlinear
115 system, even for an idealized problem, usually requires more than just pencil and paper, *viz.*, a
116 numerical code or model that serves to time-step a finite difference representation of the shallow water
117 equations. In this and in many other ways, numerical models are an essential part of atmospheric and
118 oceanic science, and for example, nearly all of the PhD students in the MIT/WHOI Joint Program
119 (Physical Oceanography) use numerical models during their thesis research. For many of these students,
120 that is also their first, hands-on experience. An implicit goal of this essay is to introduce the practice of
121 numerical modelling, especially hypothesis testing and solution interpretation, at an introductory level.
122 To that end, some of the homework assignments suggested here will require the generation of new
123 numerical solutions. Source codes that are directly applicable to these problems are available on an
124 anonymous ftp site linked in Sec. 6.3. By introducing some of the methods (and limitations) of
125 numerical research, this essay is intended to supplement the excellent GFD texts by, among others,
126 Cushman-Roisin, Gill and Pedlosky, that treat many of the same geostrophic adjustment problems via
127 mainly analytic solution methods.³

²Much of the pioneering research on the topics discussed in this essay appeared in a series of classic papers by Carl G. Rossby and colleagues published in the late 1930s. A collection of Rossby's highly readable papers is available online at <http://www.aos.princeton.edu/WWWPUBLIC/gkv/history/general.html>

³An introduction to geophysical fluid dynamics at about the level of this essay is by B. Cushman-Roisin, *Introduction to Geophysical Fluid Dynamics* (Prentice Hall, Engelwood Cliffs, New Jersey, 1994). Somewhat more advanced and highly recommended for the topic of geostrophic adjustment is A. E. Gill, *Atmosphere-Ocean Dynamics* (Academic Press, NY, 1982) and for waves generally, J. Pedlosky, *Waves in the Ocean and Atmosphere* (Springer, 2003).

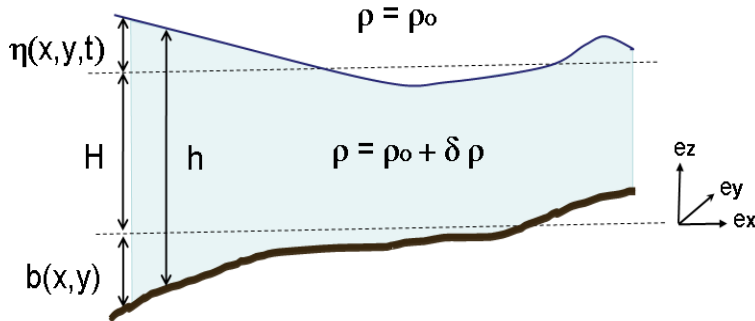


Figure 3: Schematic of a single fluid layer (light blue) sitting on a variable-depth lower, solid boundary, e.g., the sea floor. The horizontal dashed lines are level surfaces (perpendicular to gravity). This layer could be a homogeneous ocean, in which case the fluid above is the atmosphere and $\delta\rho \gg \rho_o$. In that case η is the displacement of the sea surface (as in Figs. 1 and 2). Or, it could be a relatively dense layer within a stratified ocean, in which case the fluid above is just slightly less dense, $\delta\rho \ll \rho_o$, and η is the displacement of a density surface. In either case, it is presumed that the fluid above the active layer does not impose a horizontally-varying pressure upon the active layer. Up until Sec. 4.4.3 $b = 0$, and hence the layer thickness is just $h = H + \eta$.

128 2 Shallow water model

129 The section derives the shallow water model, essentially a single fluid layer that varies in the horizontal,
 130 (x, y) , but not in the vertical, z .⁴ This layer is presumed to have a nominal thickness, H , and rests upon a
 131 lower, solid boundary, e.g., the sea floor, that is at a depth $z = -b(x, y)$ (Fig. 3). The vertical
 132 displacement of the upper surface (relative to a level surface) is $\eta(x, y, t)$ and will vary with horizontal
 133 position and with time. The thickness of the layer is $h(x, y, t) = H + b(x, y) + \eta(x, y, t)$ in general, but
 134 from here until Sec. 4.4.3 only the case $b = 0$ (flat bottom) will be considered. The fluid above is
 135 presumed to be at rest, and to have a uniform density ρ_o , and pressure, P_a , that is uniform horizontally.
 136 The fluid within the active layer has a greater density than the fluid above, $\rho_o + \delta\rho$ where $\delta\rho$ is a
 137 specified constant noted below.

138 Compared with the single parcel model of Part 1, this single layer model is a very big step toward a
 139 realistic model of the atmosphere or ocean. There are, however, two important
 140 idealizations/simplifications that facilitate both the solution and analysis, though at the expense of
 141 generality.

⁴Readers who already know the shallow water model may, of course, skip this rather lengthy section, but should take a look at Secs. 2.2 and 2.3.

142 1) **Single layer.** The horizontal velocity \mathbf{V} is implicitly depth-independent since it is represented by
 143 a two component vector field i.e., $\mathbf{V}(x, y, t) = [u(x, y, t), v(x, y, t)]$, vs. the true three-dimensional
 144 $\mathbf{V}(x, y, z, t)$, a bigger help than it may first appear. For this neglect of vertical structure to be a valid
 145 approximation, the nominal layer thickness, H , must be somewhat less than the horizontal scale of the
 146 motion, e.g., a wavelength. A single layer model of this kind is often and appropriately termed a shallow
 147 water model, even when H is taken to be the full depth of the ocean. The most convincing justification
 148 for the shallow water model comes from the analysis of a two layer model that includes both external
 149 (barotropic) and internal (baroclinic) normal modes (see the appendix to this section). The two layer
 150 model makes clear that a shallow water model is appropriate to a study of either barotropic or baroclinic
 151 normal modes, but not both at once. This is not a significant shortcoming given the broad goal of this
 152 study and, moreover, it wouldn't matter which normal mode was chosen. But given that a specific goal
 153 is to model the oceanic mesoscale eddies seen in Fig. 2, then as nominal values, $H = 500$ m and $\delta\rho = 2$
 154 kg m^{-3} , are appropriate to the baroclinic motions of the ocean's main thermocline. Ocean mesoscale
 155 eddies have a radius $L \approx 100$ km, and hence this layer thickness is indeed 'shallow' in the sense that
 156 $H/L \ll 1$. It is notable that oceanic eddies are mainly upper ocean phenomenon, i.e., strongest above
 157 the main thermocline. They certainly are not resting on the sea floor, as does the single layer model
 158 derived here. The reduced gravity approximation discussed in Sec. 2.4.3 shows that such a single layer
 159 model will be most appropriate provided that the gravity wave speed of the model is equal to the gravity
 160 wave speed of the baroclinic eddies of interest (and the sea floor is taken to be flat). If the intent was to
 161 utilize the shallow water model to make a realistic simulation of a given, observed flow phenomenon,
 162 then three additional approximations or simplifications would have to be valid: 1) that the initial state
 163 was free of vertical shear, $\partial\mathbf{V}/\partial z = 0$, 2) that the fluid of interest was outside of frictional boundary
 164 layers, and 3) that the horizontal density variation within the layer was effectively zero. Most real
 165 geophysical flows violate all three of these conditions to some degree, especially 1) and 3). A realistic
 166 simulation is likely to require greater resolution in the vertical, e.g., some number of shallow layers
 167 stacked one on top of another to represent vertical shear, boundary layers, stratification, etc. However,
 168 consistent with the inductive method laid down in Part 1, one layer will be enough for us, for now.

169 2) **Ideal fluid.** The physical processes allowed into this model are those of an ideal fluid, *viz.*,
 170 hydrostatic pressure and transport by the fluid flow. The wide range of physical processes associated
 171 with the thermodynamic properties of a real fluid, e.g., compressibility, diffusion and viscosity, are
 172 omitted. This too may seem a bit high-handed, but is consistent with building the simplest model that
 173 will help us understand some of the consequences of Earth's rotation. An external \mathbf{F} is allowed in, but is
 174 treated as a body force rather than a boundary stress.

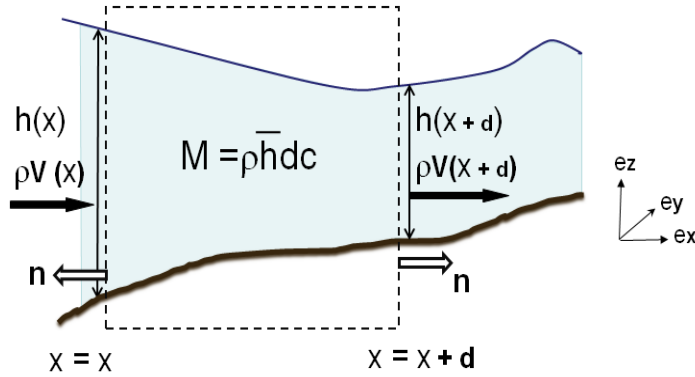


Figure 4: A control volume defined by thin dashed lines. The average thickness is \bar{h} , the length is d , and the width in the y -direction is c (y is normal to the page and is not shown). The statement of mass conservation appropriate to the problems considered here is that the mass of the active layer within the control volume, M , can change only because of mass fluxes due to fluid flow normal to the sides of the control volume, $-\rho A \mathbf{V} \cdot \mathbf{n}$, where A is the area. The layer thickness variation shown here is exaggerated; changes of layer thickness of even a few percent can be significant.

175 2.1 Mass and momentum balance of an ideal fluid layer

176 **Mass Conservation:** The starting point is the assertion that mass (volume, really, since density is
 177 presumed constant) can be neither created nor destroyed by classical fluid dynamical processes. The
 178 positive assertion of this is that the mass of the layer at a given point can change only by virtue of mass
 179 fluxes associated with the (horizontal) fluid velocity within the layer. This is oftentimes referred to as
 180 the continuity requirement.

181 To find the corresponding mathematical form of this physical assumption, the mass balance will be
 182 evaluated over a control volume that spans the full thickness of the layer, Fig. (4). The mass of the layer
 183 contained within the control volume is

$$184 \quad M = \bar{\rho} \bar{h} d c, \quad (1)$$

185 where $\bar{\rho}$ is the constant density within the layer, and \bar{h} is the average thickness over the interval x
 186 $x + d$ and c is the width (the dimension into the page). The mass flux due to fluid flow through a given
 187 surface of area A is just

$$188 \quad \text{mass flux} = -\rho A \mathbf{V} \cdot \mathbf{n}, \quad (2)$$

189 where \mathbf{n} is the outward unit normal of the surface. For the left-facing side of the control volume in Fig.
 190 (4), $\mathbf{n} = (-1, 0, 0)$ and the mass flux = $\rho h c u$, where u is the x -component of the fluid velocity and $h c$ is

191 the area. These are evaluated at the x of the left-facing side. Noting that the unit normal on the
 192 right-facing side at $x + d$ is $\mathbf{n} = (1, 0, 0)$, then the sum of the mass fluxes through both x -facing sides is

$$193 \quad \frac{\partial M}{\partial t} = \rho(h(x)u(x) - h(x+d)u(x+d))c. \quad (3)$$

194 By our construction of mass conservation, this net mass flux is equal to the time rate of change of mass
 195 within the control volume. The mass $M(x, y, t)$ varies with position and time, but notice that the time
 196 derivative of (3) is a partial derivative, since M is the mass of a control volume that is fixed in space.
 197 Inserting the definition of M , and dividing through by ρ , c and d gives

$$198 \quad \frac{\partial \bar{h}}{\partial t} = \frac{1}{d}(h(x)u(x) - h(x+d)u(x+d)).$$

199 Now let d go to zero, and the right-hand side also becomes a partial derivative

$$200 \quad \frac{\partial h}{\partial t} = -\frac{\partial(hu)}{\partial x}, \quad (4)$$

the one-dimensional, differential statement of mass conservation (though since the constant density and
 area are divided out, the units are length per time). Thus, the mass inside the control volume will
 change if and only if there is a *divergence* of the mass flux associated with the fluid flow; the mass flux
 alone is not relevant insofar as the M at a given position is concerned. Had variations in the y -direction
 (normal to the page) been considered, then there would arise an additional term, $-\partial(hv)/\partial y$, and the
 two-dimensional form of mass conservation for a shallow water model is

$$\frac{\partial h}{\partial t} = -\left(\frac{\partial(hu)}{\partial x} + \frac{\partial(hv)}{\partial y}\right) \quad (5)$$

$$= -\nabla \cdot (h\mathbf{V}). \quad (6)$$

201 This way of writing mass conservation is sometime said to be the flux form or conservative form, and is
 202 generally preferred for implementation in a numerical model. For purposes other than numerical
 203 integration it may be useful to expand the divergence operator and combine the partial time derivative
 204 and the advection term into the material derivative,

$$205 \quad \frac{D(\)}{Dt} \equiv \frac{\partial(\)}{\partial t} + u\frac{\partial(\)}{\partial x} + v\frac{\partial(\)}{\partial y}, \quad (7)$$

206 about which more below. The mass balance (thickness balance) written using the material derivative is

$$207 \quad \frac{Dh}{Dt} = \frac{\partial h}{\partial t} + u\frac{\partial h}{\partial x} + v\frac{\partial h}{\partial y} = -h\left(\frac{\partial u}{\partial x} + \frac{\partial v}{\partial y}\right). \quad (8)$$

208 **Momentum conservation:** At a given point, the momentum of the layer $\rho h\mathbf{V}$, can change only by a
 209 relative few prescribed processes, by momentum fluxes associated with the fluid velocity, by pressure

210 variations, and by the Coriolis force, an inertial force that acts throughout the body of the fluid. There
 211 may also be an external force, \mathbf{F} , (not to be confused with the lower case f) that acts as a stress, a
 212 tangential force per area on the upper or lower boundaries.

213 The x component of momentum (per unit area) is ρhu , and the momentum flux due to the
 214 x -component of the velocity is just ρhu^2 , which, notice, is proportional to kinetic energy. The pressure
 215 flux can be computed given the known density and layer thickness, and presuming that the vertical
 216 accelerations of the motion are very, very small compared to the acceleration of gravity, $\frac{\partial^2 h}{\partial t^2} \ll g$. In
 217 that case the vertical component of momentum balance is the hydrostatic pressure relation,

$$218 \quad \frac{\partial p}{\partial z} = -g\rho,$$

219 and the hydrostatic pressure within the layer ($z < h$) is

$$220 \quad P(x, y, z) = P_a(z) - g\rho_0 z + g\delta\rho(h(x, y, t) - z). \quad (9)$$

221 $P_a(z)$ is the z -dependent but horizontally uniform pressure in the fluid above the active layer and the
 222 second term on the right is the hydrostatic pressure due to the constant density ρ_0 . Neither of these
 223 z -dependent terms contribute to horizontally-varying momentum fluxes and may be ignored in what
 224 follows. The third term represents the pressure anomaly associated with the horizontally-varying layer
 225 thickness, h and notice that a relatively large layer thickness indicates a high pressure anomaly within
 226 the layer. The momentum flux due to the anomaly of hydrostatic pressure on an x -facing side of the
 227 control volume having width c is then

$$228 \quad g\delta\rho c \int_0^h (h-z) dz = g\delta\rho c \frac{h^2}{2}.$$

229 The x -component momentum flux on an x -facing side thus has two terms:

$$230 \quad \text{momentum flux} = \rho chu^2 + g\delta\rho c \frac{h^2}{2}. \quad (10)$$

231 The first term on the right is the flux of u -momentum due to the u -component of the velocity and so is
 232 proportional to u^2 , and the second term is the layer-averaged anomaly of the hydrostatic pressure $\propto h/2$
 233 acting over the face of the control volume, ch . When the body force due to the Coriolis force is included,
 234 $-\mathbf{f} \times \mathbf{V} = (fv, -fu)$, and when the operations noted above to go from Eqn. (3) to Eqn. (6) are repeated
 235 here, the conservative (or flux) form of the shallow water momentum (per mass \times area) equations are

$$236 \quad \frac{\partial(hu)}{\partial t} = -\frac{\partial(huv)}{\partial y} - \frac{\partial(hu^2 + \frac{1}{2}g'h^2)}{\partial x} + fhv + F_x, \quad (11)$$

$$237 \quad \frac{\partial(hv)}{\partial t} = -\frac{\partial(huv)}{\partial x} - \frac{\partial(hv^2 + \frac{1}{2}g'h^2)}{\partial y} - fhu + F_y, \quad (12)$$

239 where $g' = g\delta\rho/\rho$ is the reduced gravity (also buoyancy per unit volume). If the upper surface of the
 240 layer is the sea surface, then $\delta\rho \approx \rho$, and $g' \approx g$; if the upper surface is within the comparatively
 241 weakly stratified ocean, then $\delta\rho \ll \rho$ and so $g' \ll g$. Unless assumed otherwise for modelling purposes,
 242 the f of these equations varies with latitude. The consequences of rotation, represented here by the
 243 Coriolis force, are the central theme of this essay.

244 The external force shown here as $\mathbf{F} = (F_x, F_y)$ could represent wind stress, in which case we would
 245 probably say that $\mathbf{F} = \mathbf{F}(x, y)$ is a specified function of space only. Or, it could represent a bottom drag,
 246 in which case $\mathbf{F} \propto -r\mathbf{V}$ as in the single parcel model of Part 1. Notice that F must have dimensions of
 247 force/mass, though it will be referred to as 'force'. Our main interest here is what the fluid itself does,
 248 rather than \mathbf{F} , and so unless it is noted otherwise, presume that $\mathbf{F} = 0$.

249 The shallow water mass and momentum balances written using the material derivative are then
 250 (repeating Eqn. 8),

$$251 \quad \frac{Dh}{Dt} = \frac{\partial h}{\partial t} + u\frac{\partial h}{\partial x} + v\frac{\partial h}{\partial y} = -h\left(\frac{\partial u}{\partial x} + \frac{\partial v}{\partial y}\right), \quad (13)$$

$$252 \quad \frac{Du}{Dt} = \frac{\partial u}{\partial t} + u\frac{\partial u}{\partial x} + v\frac{\partial u}{\partial y} = -g'\frac{\partial h}{\partial x} + fv + \frac{F_x}{h}, \quad (14)$$

$$253 \quad \frac{Dv}{Dt} = \frac{\partial v}{\partial t} + u\frac{\partial v}{\partial x} + v\frac{\partial v}{\partial y} = -g'\frac{\partial h}{\partial y} - fu + \frac{F_y}{h}. \quad (15)$$

254 The vector equivalents are

$$255 \quad \boxed{\frac{Dh}{Dt} = \frac{\partial h}{\partial t} + \mathbf{V} \cdot \nabla h = -h\nabla \cdot \mathbf{V}} \quad (16)$$

$$256 \quad \boxed{\frac{D\mathbf{V}}{Dt} = \frac{\partial \mathbf{V}}{\partial t} + \mathbf{V} \cdot \nabla \mathbf{V} = -g'\nabla h - f\mathbf{k} \times \mathbf{V} + \frac{\mathbf{F}}{h}} \quad (17)$$

257 It is useful to pause for a moment and consider how these shallow water equations (17) compare
 258 with the equation of motion appropriate to the single *parcel* of Part 1, Sec. 5 (repeated here but omitting
 259 the bottom friction term from the latter and ignoring \mathbf{F} of the former),

$$260 \quad \frac{d\mathbf{V}}{dt} = g'\nabla b - f\mathbf{k} \times \mathbf{V}.$$

261 1) The Coriolis terms are identical in the two systems. The Coriolis force is an inertial force
262 that depends solely upon the fluid velocity relative to the rotation vector, and makes no
263 distinction of the physical properties of the material. And, of course, absent that
264 fundamental property, it would not have been appropriate to use a single parcel model as
265 the starting point in Part 1.

266 2) The pressure gradient term of the shallow water model, $-g'\nabla h$, has the form of the
267 buoyancy force on a dense parcel sitting on a slope, $g'\nabla b$ (sign aside). A crucial difference
268 is that the bottom slope of the single parcel model is prescribed and fixed, while the
269 gradient of layer thickness in the shallow water model is a dependent variable, dependent
270 upon space and time via the mass balance, Eqn. (16). Mass balance has no counterpart in
271 the single parcel model. In an ideal fluid model such as this one, the variable pressure is the
272 only way that a fluid parcel interacts with the rest of the fluid domain. For example, if fluid
273 begins to pile up (converge) at a given location, then the layer thickness and the hydrostatic
274 pressure will go up until the pressure gradient is sufficient to push fluid away from that
275 location. The rate at which the fluid responds to a convergence determines the speed of
276 gravity wave propagation (Sec. 3.1).

277 3) The time derivatives have quite different meanings implicit in the use of different
278 symbols: the ordinary time derivative d/dt of the single parcel model is the time rate
279 change of a specific, material parcel, which in a fluid dynamics context would often be
280 termed a Lagrangian coordinate system. Different parcels have different initial conditions
281 and subsequent forcing, and to solve for a fluid flow requires solving for many such
282 (interacting) parcels. The material derivative D/Dt of the present shallow water model is
283 equal to the time rate of change following a moving parcel at the instant the parcel is
284 coincident with the spatial position where D/Dt is evaluated. The independent coordinates
285 of our shallow water model are fixed spatial coordinates and time, which in fluid dynamics
286 is often referred to as an Eulerian coordinate system. The fluid present at a fixed location
287 changes due in part to the fluid flow via the advection process represented by the term
288 $\mathbf{V}\cdot\nabla(\)$. Advection is the product of two dependent variables, velocity times thickness
289 gradient in Eqn. (16) or velocity times the velocity gradient in Eqn. (17) and so is nonlinear.
290 Advection and this associated nonlinearity are right at the heart of fluid dynamics and are a
291 significant reason why numerical methods and numerical models are essential tools of
292 atmospheric and oceanic sciences.

2.2 Solving and diagnosing the shallow water system

Equations (16) - (35) are a coupled set of nonlinear, partial differential equations in three dependent variables, the two components of the horizontal velocity, $\mathbf{V} = (u, v)$, and the thickness, h . The parameters g and $\delta\rho$ are constants for any given problem, and the Coriolis parameter f is a specified function of the north-south coordinate, y , including in one experiment $f = 0$, about which much more below.

The shallow water model is nonlinear because of the advection terms of the material derivative noted above, e.g., the east-west advection of north-south momentum is $u \partial v / \partial x$, which is the product of two dependent variables. Solutions of a shallow water system including these nonlinear terms are necessarily generated by numerical methods: the one-dimensional experiments shown here were solved by the Matlab script `geoadj_1d.m`, and the two-dimensional experiments by the Fortran code `geoadj_2d.for`, both of which are linked in Sec. 6.3.⁵

In common with any numerical model, these models produce (putative) solutions in the form of very large data files, $u(x_i, y_i, t_j), v(x_i, y_i, t_j), \dots$, where x_i, t_i are discretized position and time. To verify that this mass of data is faithful to the model equations and to the boundary/initial conditions, and then to go on and learn something useful requires as much thought and effort as does generating the model and solution in the first place. To wit, we will seek to 1) construct useful visualizations of the solutions (this can be the artful side of numerical modelling), 2) diagnose the balances of energy and potential vorticity, 3) interpret the wave-like properties of the solution using the dispersion relation of the corresponding, linearized system, and then 4) form and test hypotheses regarding parameter dependence by conducting further numerical experiments (that will be the homework, actually).

2.2.1 Wave velocities and fluid velocities

A qualitative difference between a shallow water model and the single parcel model of Part 1 is that a shallow water model supports wave motions — relatively fast-moving gravity waves will arise in all of our experiments, and much lower frequency Rossby waves will arise when there is a north-south variation of f (deferred to Part 3). If the layer thickness anomaly is a simple harmonic motion varying with x and t only, $\eta(x, t) \propto \eta_o \sin(kx - \omega t)$, then a constant phase propagates at the rate of the

$$\text{wave phase speed, } C_p = \frac{\omega}{k}, \quad (18)$$

⁵The details of the numerical methods are all-important in setting the efficiency and the accuracy of the solutions, but not something that will be discussed here. An excellent, concise reference on numerical methods suitable for the shallow water model is <http://www.mathworks.com/moler/exm/chapters/water.pdf>

321 where wave frequency is $\omega = 2\pi/(\text{wave period})$, or waves per time, and the wavenumber is
 322 $k = 2\pi/(\text{wave length})$, or waves per space interval. This wave propagation velocity is often readily
 323 apparent (as in the cover graphic). In many cases the thickness anomaly will be the result of a
 324 superposition of waves, i.e., waves of different wave numbers and frequencies, and in that case the
 325 envelope of the superposition will move at the

$$326 \quad \text{wave group speed, } C_g = \frac{\partial \omega}{\partial k}, \quad (19)$$

327 This makes clear that the dispersion relation, $\omega(k)$, is going to be very important. The dispersion
 328 relation is determined by the physics of the wave medium, specifically the relationship of restoring
 329 force to wavelength. This differs greatly between pure gravity waves (Sec. 3.1), gravity waves in the
 330 presence of rotation (Sec. 3.2), and Rossby waves (Part 3). The motion of the fluid is, in general,
 331 qualitatively different from the phase speed of waves that may be propagating through the fluid. Fluid
 332 velocity is usually much less than the gravity wave speed and is often much greater than the Rossby
 333 wave speed (Rossby waves in Part 3). To see the fluid motion one can simply plot the field of the
 334 instantaneous velocity vectors, which shows the

$$335 \quad \text{Eulerian fluid velocity : } \mathbf{V}(x_i, y_i, t_j) = (u(x_i, y_i, t_j), v(x_i, y_i, t_j)), \quad (20)$$

336 at the fixed positions (x_i, y_i) and the times, t_j . This Eulerian velocity field is the direct output of the
 337 numerical model, useful in itself, and the starting point for much else. The fluid velocity is generally
 338 proportional to the amplitude of the motion; in the problems discussed here, $V \propto \eta_o$, where η_o is the
 339 initial interface displacement. Wave speeds, on the other hand, are independent of amplitude in linear
 340 approximation, and generally only weakly dependent upon amplitude in nonlinear models (more on this
 341 below).

342 To see the transport of fluid over a long term we can compute the evolution of a passive tracer, say
 343 s , that is carried along with the flow without in any way altering the flow. This tracer may be embedded
 344 in the fluid at the starting time, $s_o = s(x, y, t_o)$ in any way that will serve to highlight the features of
 345 interest. This tracer is then presumed to be conserved following the flow,

$$346 \quad \frac{Ds}{Dt} = 0, \quad (21)$$

347 or, expanding the material derivative,

$$348 \quad \frac{\partial s}{\partial t} = -\left(u \frac{\partial s}{\partial x} + v \frac{\partial s}{\partial y}\right) = -\mathbf{V} \cdot \nabla s. \quad (22)$$

349 The tracer value at a fixed location will thus change in time due solely to advection by the flow.
 350 Diffusion of tracer is omitted in this ideal fluid model, though some inadvertent 'numerical diffusion'
 351 will always be present in numerical solutions. Thus Eqn. (21) would hold exactly only in a perfect
 352 numerical solution (and you may never see one).

353 The trajectories of discrete fluid parcels, or 'floats', make a useful complement to the continuous
 354 tracer. The trajectory of the i th float, (x^i, y^i) , is found by integrating the (Eulerian) fluid velocity at the
 355 moving location of the float,

$$356 \quad x^i(t) = x_o^i + \int_{t_o}^t u(x^i, y^i, t) dt \quad \text{and} \quad y^i(t) = y_o^i + \int_{t_o}^t v(x^i, y^i, t) dt. \quad (23)$$

357 Which specific fluid parcel or float is being tracked in this way is given by the initial position, i.e., the
 358 i th float starts at $x_o^i = x^i(t = t_o)$. The float will likely be found between the discrete grid points of the
 359 numerical model's Eulerian velocity field and so in practice this will require some interpolation. The
 360 trajectory is the fundamental dependent variable of a Lagrangian description (rather than the velocity as
 361 in the Eulerian description). But if needed, the Lagrangian velocity may be computed from the
 362 trajectories via

$$363 \quad \text{Lagrangian fluid velocity:} \quad \mathbf{U}^i(t) = \left(\frac{\partial x^i(t)}{\partial t}, \frac{\partial y^i(t)}{\partial t} \right). \quad (24)$$

364 Tracer evolution by advection Eqn. (21) and float trajectories by Eqn. (23) are very closely related, and,
 365 for example, the tracer concentration at the moving location of a float should be exactly conserved
 366 (numerical diffusion and tracking errors aside).

367 The relationship between the Eulerian and the Lagrangian velocities depends very much upon the
 368 length of time that a float is tracked, the $t = t_o + \Delta t$ of Eqn. (23). If Δt is so brief that the float moves
 369 only an infinitesimal distance compared to the scale over which the Eulerian velocity varies in space,
 370 then the Lagrangian velocity will converge to the Eulerian velocity at the starting point. Much more
 371 interesting is the case that Δt is very long, in Part 3 up to a year, in which case any given float may
 372 wander into regions having very different Eulerian velocity, which is also likely changing in time. In
 373 that event, and aside from special cases, the Lagrangian velocity will likely bear no simple relationship
 374 to the Eulerian velocity.

375 2.2.2 Energy balance

376 Energy conservation is a fundamental physical law that can sometimes be of use in analyzing a fluid
 377 flow, especially if, as here, dissipation and thermal (internal) energy may be neglected. In that case the
 378 mechanical energy, $E = KE + PE$, is conserved, where E is the sum of kinetic energy (per unit mass),
 379 $KE = \frac{1}{2}h\mathbf{V}^2$, and potential energy (per unit mass), $PE = g' \int_0^\eta z dz = \frac{1}{2}g'\eta^2 + const$. To find the rate of
 380 change of KE , take the dot product of the momentum equation with the velocity times thickness, and
 381 the rate of change of PE is found by multiplying the continuity equation by the thickness anomaly times
 382 reduced gravity. The mechanical energy balance is

$$383 \quad \boxed{\frac{DE}{Dt} = -g'\nabla \cdot (\eta h \mathbf{V}) + \mathbf{F} \cdot \mathbf{V}} \quad (25)$$

384 The flux term on the right-hand side is the product of pressure anomaly, thickness and velocity, i.e.,
385 pressure work (actually, pressure work rate, or power). For example, if the pressure anomaly is positive
386 on the (imaginary) boundary of a control volume where the velocity is directed outward, say, then the
387 fluid inside the control volume will do pressure work on the fluid outside of the control volume. The
388 energy within the control volume will thus decline, while the energy outside the control volume will
389 increase. The pressure-work term thus accounts for the outward energy transport associated with wave
390 radiation through an open boundary, for example. The fluid flow can also transport energy at the rate \mathbf{V} ,
391 a process accounted by the advection term, $\mathbf{V} \cdot \nabla E$, of the total derivative. Finally, note that an external
392 force \mathbf{F} can either increase or decrease energy depending upon whether it has a component parallel or
393 anti-parallel to the fluid velocity.

394 2.2.3 Potential vorticity balance

395 Throughout Part 1, our perspective on dynamics was through the *linear* momentum balance (linear here
396 in the geometric sense), and rotation appeared by way of the Coriolis *force*. That was all that was
397 possible given a single parcel model. Momentum balance is always relevant, but may not always be
398 highly revealing. Given the present fluid model, there is another and complementary point of view,
399 *angular* momentum balance, that has proven immensely fruitful for understanding some of the most
400 important low frequency (frequencies less than f) phenomena of geophysical fluid dynamics. Two main
401 reasons, to get a little ahead in this short story, are that 1) Earth's rotation provides a very large
402 background angular momentum that is made visible by small changes in the thickness or latitude of a
403 fluid column, and, 2) the angular momentum balance amounts to a kind of filter that eliminates high
404 frequency gravity wave motions and so serves to highlight the processes that cause departures from
405 geostrophic balance and that lead to low frequency currents and winds, i.e., large scale circulation.

406 Back a step or two..... to analyze the motion of a rotating, solid object, say a gyroscope, you might
407 begin by computing the linear momentum balance of the component pieces. This would require an
408 accounting of radial accelerations and internal stresses on each piece and would likely be a fairly
409 arduous task. Assuming that the gyroscope is not at risk of breaking up, then at some point you might
410 decide to take the structure for granted, and focus your effort toward analyzing the angular (azimuthal)
411 momentum balance of the gyroscope as a whole. As a first step you would define a coordinate system
412 that gave the most compact and least complex accounting of the moment of inertia of the gyroscope and
413 then consider the processes that cause the angular momentum to change with time. The physical
414 content of your angular momentum analysis would not be fundamentally different from the linear
415 momentum description, but it would likely be a great deal simpler in the same way that choosing
416 appropriate variables and an appropriate coordinate system can facilitate any mathematical analysis.
417 The same considerations apply to an analysis of a fluid flow: as we will see in examples here, an
418 angular momentum analysis and description will often (but not always!) be a good deal simpler and so

419 provide a great deal more insight than does the otherwise equivalent linear momentum analysis.

420 The fluid flow equivalent of angular velocity is the curl of the fluid velocity,

$$421 \quad \boxed{\xi \equiv \nabla \times \mathbf{V}}$$

422 called the vorticity. If the fluid velocity is a three-dimensional vector, then the vorticity is also a
423 three-dimensional vector. In the special case of the shallow water model, the velocity varies only in the
424 two horizontal dimensions, and so the shallow water vorticity,

$$425 \quad \xi = \nabla \times \mathbf{V} = \left(\frac{\partial v}{\partial x} - \frac{\partial u}{\partial y} \right)_z, \quad (26)$$

426 has a vertical component only and is effectively a scalar. You can visualize vorticity as the rotation of
427 small (but not quite point-like) two-dimensional parcels, e.g., cylinders, that make up the fluid.⁶ As we
428 will see, however, vorticity in a plane wave will arise from horizontal shear in the direction normal to
429 the velocity, e.g., $\xi = \partial v / \partial x$ or $\xi = -\partial u / \partial y$ are quite possible, and so spinning cylinders are not
430 always apropos. If the direction of rotation is the same as Earth's rotation, the vorticity is said to be
431 *cyclonic* (from the Greek *kyklon*, for circular motion). Cyclonic rotation is thus counterclockwise in the
432 northern hemisphere and clockwise in the southern hemisphere. Anticyclonic is the reverse. Notice that
433 vorticity has units of inverse time, or frequency, the same as the Coriolis parameter, f . There is an
434 important sense in which ξ may be compared to and even added to f , as discussed below.

The vorticity of a fluid is unlike the angular momentum associated with a solid object in that it is defined at every point in a fluid, i.e., in principle there is a vorticity field that accompanies every fluid flow (although it could be zero), just as there is a velocity field and a thickness field in the shallow water model. The governing equation for this vorticity field may be found by taking the curl of the momentum equation, $\partial / \partial x$ of the y -component minus $\partial / \partial y$ of the x -component. A consequence of applying the curl operator is that all of the forces that are derivable from a potential are eliminated, most notably the pressure gradient in the shallow water model, i.e.,

$$\nabla \times \nabla(\eta(x, y)) = \frac{\partial^2 \eta}{\partial x \partial y} - \frac{\partial^2 \eta}{\partial y \partial x} = 0.$$

435 A divergence term $\partial u / \partial x + \partial v / \partial y$ will arise and may be eliminated using the thickness (continuity)
436 equation, (16). After a little further rearrangement, the result is a balance equation for a scalar, q , called
437 the potential vorticity,

$$438 \quad \boxed{\frac{Dq}{Dt} = \frac{\partial q}{\partial t} + \mathbf{V} \cdot \nabla q = \frac{1}{h} \nabla \times \frac{\mathbf{F}}{h}} \quad (27)$$

⁶An essential resource for all students of fluid mechanics is the collection of fluid mechanics films made in the 1960s by Ascher Shapiro and colleagues and now available online at <http://web.mit.edu/hml/ncfmf.html> Today these seem a little old-fashioned, but nevertheless provide excellent visualizations of many key concepts, including vorticity and Eulerian and Lagrangian coordinate systems that are timeless; these films are very highly recommended. A more modern film collection, many of which emphasize rotational effects, is <http://planets.ucla.edu/featured/spinlab-geoscience-educational-film-project/>

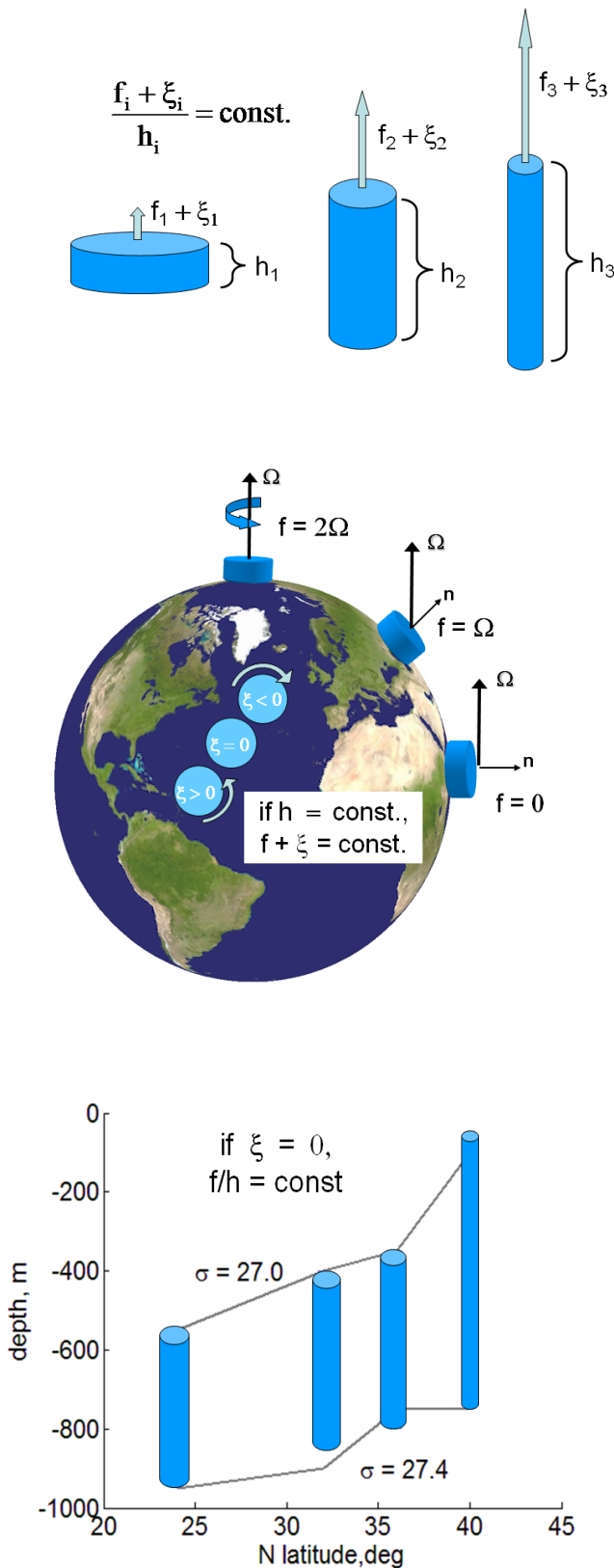


Figure 5: Some illustrations of q -conservation, $Dq/Dt = 0$, by fluid columns that have a constant volume but may have a variable thickness, h and that are free of external torques, $\nabla \times \mathbf{F} = 0$. **(upper)** If h is variable, then the absolute vorticity, $f + \xi$, will change in proportion to h . This is true whether the absolute vorticity $\approx \xi$, because $f \ll \xi$ as in small scale or engineering flows, or if $\xi \ll f$ and ξ is effectively zero, as in a gyre-scale flow, illustrated in the lower panel. **(middle)** The columns perched at upper and right on the Earth are intended to show that the planetary vorticity due solely to Earth's rotation is given by $\nabla \times \mathbf{V}_\Omega = 2\boldsymbol{\Omega} \cdot \mathbf{n} = 2\Omega \sin(\text{latitude}) = f$. The planetary velocity \mathbf{V}_Ω and thus the planetary vorticity f are apparent to an inertial observer, implicit in this view from space. We Earth-bound observers will see only the relative velocity \mathbf{V} , i.e., winds and ocean currents, and the relative vorticity, ξ . The planetary vorticity is not directly observable (though the stars turning overhead are a mirror image). The three columns in the North Atlantic are shown end-on to illustrate the sense of relative vorticity that would be acquired by a q -conserving column that was displaced north or south away from a reference site where $\xi = 0$ while holding h constant. This and the next mechanism involve $f(\text{latitude})$ that will be taken up in Part 3. **(lower)** If the relative vorticity ξ is much, much less than f and remains effectively zero, as in a gyre-scale flow, then a change in the latitude of a column will be accompanied by a change in the thickness of a column in the sense shown here, i.e., smaller h in the direction of smaller $|f|$. The solid lines are depths of the 27.0 and 27.4 potential density surfaces along a plausible trajectory through the main thermocline of the eastern subtropical North Atlantic. These data are after Fig. 4 of Luyten J. R. et al., 1983: 'The ventilated thermocline', *J. Phys. Oceanogr.* 13, 292 - 309.

439 where

$$440 \quad q = \frac{f + \xi}{h} \quad (28)$$

441 Up until Part 3 our interest will be the fluid only, $\mathbf{F} = 0$, in which case we have a q -conservation law

$$442 \quad \frac{Dq}{Dt} = 0 \quad (29)$$

443

444 The terms in potential vorticity balance are:

445 $\xi = \nabla \times \mathbf{V}$ is often called the *relative* vorticity in this context, since it is the vorticity of the
 446 relative velocity, i.e., the winds and currents observed from an Earth-attached reference
 447 frame. In Part 1, Sec. 4 the relative velocity was denoted by \mathbf{V}' , though by now the prime
 448 superscript has been dropped.

449 $f = \nabla \times \mathbf{V}_\Omega$ is the *planetary* vorticity of the planetary velocity, $\mathbf{V}_\Omega = \boldsymbol{\Omega} \times \mathbf{X}$, due to Earth's
 450 rotation, Fig. (5), where \mathbf{X} is the position vector (Sec. 4.3, Part 1). f may be written in
 451 several forms, $f = \nabla \times \boldsymbol{\Omega} \times \mathbf{X} = 2\boldsymbol{\Omega} \cdot \mathbf{n} = 2\Omega \sin(\text{latitude})$,

452 $f + \xi = \nabla \times (\mathbf{V}_\Omega + \mathbf{V})$ is appropriately termed the *absolute* vorticity, since it is indeed the
 453 vorticity of the absolute velocity, $\mathbf{V}_\Omega + \mathbf{V}$, i.e., the velocity that would be observed from an
 454 inertial reference frame, and finally,

455 h is the layer (or column) thickness.

456 The conservation equation (29) states that q is conserved following an ideal fluid parcel (or fluid
 457 column since this is a single layer model). By ideal we mean that there is no external torque due to wind
 458 stress or bottom friction. What is most important is to notice what is missing from (29): there is no
 459 process comparable to pressure work found in the energy balance, Eqn. (25), that transmits energy at
 460 the speed of gravity waves — q is transported with the fluid, exactly as a passive tracer, Eqn. (21), and
 461 not at the gravity wave velocity as is energy. Thus the potential vorticity of an ideal fluid has the
 462 conservation property of a tracer (or dye) that, once put into a fluid, remains with the fluid no matter
 463 how complex the flow may be. This includes during the process of geostrophic adjustment. But unlike a
 464 passive tracer, the potential vorticity includes an important part of the velocity field, the part having
 465 relative vorticity. In some cases it may be sufficient to calculate the evolution of a flow from
 466 q -conservation only, the steady state of an adjustment process is an important example in Sec 4.4, which

467 is a marked simplification over solving the full shallow water system. However, the pure gravity wave
 468 experiment in Sec. 3.1 will show that q conservation can be irrelevant if the dynamics is such that there
 469 is no vorticity.

470 Potential vorticity is a generalized angular momentum insofar as it accounts for a variable moment
 471 of inertia (variable thickness) as well as the planetary vorticity f due to Earth's rotation. The planetary
 472 vorticity is extremely important in this regard, because f is considerably larger than is the ξ of large
 473 scale flows, usually by a factor of 10 and often much more. A fluid column having potential vorticity
 474 will exhibit a kind of gyroscopic rigidity in the sense that it will respond to changes in the parcel
 475 configuration (thickness) or to changes in latitude and thus f . For example, suppose that a fluid column
 476 has absolute vorticity $(f_1 + \xi_1)$ and thickness h_1 in an initial state, and is then stretched from h_1 to h_2 .
 477 Assuming that the stretching occurs without frictional or external torques, then the conservation law
 478 (29) applies and the absolute vorticity of the column will change to $(f_2 + \xi_2) = (f_1 + \xi_1)h_1/h_2$ (Fig. 5).
 479 Whether the change in absolute vorticity is due mainly to a change in the relative vorticity or due to a
 480 change in the planetary vorticity (latitude) can not be told without some additional information;
 481 sometimes knowing just the horizontal scale of the motion will suffice (Sec. 2, Part 3).

482 You may be wondering why we should make such a fuss over potential vorticity when the
 483 numerical model solves the more general shallow water equations. It is true that the winds or currents
 484 that might be inferred from a q -conservation argument can always be computed by the shallow water
 485 model and so q -conservation is redundant insofar as computation alone is concerned. The value of
 486 potential vorticity becomes evident when it is time to describe, interpret and understand a numerical
 487 model solution or a set of field observations: a potential vorticity-based description will often be
 488 simpler and yield far more insight than would the corresponding momentum plus continuity description.
 489 Of course, this presumes that potential vorticity concepts are a part of our working, fluid dynamics
 490 vocabulary. We can take a useful step in that direction by using potential vorticity balance to help
 491 describe and interpret the geostrophic adjustment experiments that follow in Sec. 4 and in Part 3.⁷

⁷Before ending this discussion it should be noted that the shallow water potential vorticity is not the most general form of potential vorticity, just as the shallow water model is not the most general fluid model. If the fluid velocity is a three component vector, which it generally is in the ocean and atmosphere, then so too is the vorticity. The three-dimensional vorticity equation includes a term that represents a change in the direction of the vorticity vector, e.g., from the horizontal into the vertical, often called 'tipping'. If the fluid flow is baroclinic, which the atmosphere and ocean generally are, then there is an additional term that arises from the cross-product of the density and pressure gradients, called the 'solenoidal' term. The corresponding three-dimensional and baroclinic potential vorticity that takes account of these additional processes is often called the Ertel potential vorticity; it reduces to the shallow water potential vorticity when the flow is appropriately two-dimensional and barotropic. By and large, the simpler shallow water potential vorticity will be adequate for an analysis of most large (horizontal) scale phenomenon, e.g., gyre-scale flows and even mesoscale eddies, once they are formed. However, it will not be adequate for analysis of small scale phenomenon, e.g., boundary layer roll vortices and three-dimensional turbulence. Knowing where this transition may occur requires a thorough understanding of Ertel potential vorticity. A valuable discussion of some of these more advanced concepts is available online <http://www.atm.damtp.cam.ac.uk/mcintyre/papers/ENCYC/epv-times.pdf>

492 2.2.4 Linear and nonlinear; finite amplitude effects

493 The phrases 'nonlinear' and 'finite amplitude' are often used interchangeably. Here, however, linear and
 494 nonlinear will be reserved for model equations, which are either one or the other with no gradation. The
 495 shallow water system is nonlinear because of the six terms that are the products of dependent variables,
 496 e.g., in the thickness equation (13) the terms $u\partial h/\partial x$ and $h\partial u/\partial x$ are nonlinear and so the model
 497 system is nonlinear when these are retained.⁸

498 Finite amplitude effects are the departures from linear dependence upon amplitude. Finite
 499 amplitude effects do not arise in the solution of a linear model, and are a matter of degree in the solution
 500 of a nonlinear model. For example, in the problems studied here, the amplitude is largely determined by
 501 η_o , the initial thickness anomaly. If the shallow water equations were linear (they aren't) then the
 502 solution $\eta(x, y, t)/\eta_o$ would be invariant to changes in η_o . Even in a nonlinear model, we can expect
 503 that $\eta(x, y, t)/\eta_o$ should be invariant to η_o in the limit of very small η_o (say $\eta_o = 1$ m with $H = 500$ m)
 504 simply because the nonlinear terms noted above will be very, very small compared to the dominant
 505 linear terms. The amplitude of the base case, $\eta_o = 50$ m, has been chosen to correspond with the
 506 observed SSH signature of mesoscale eddies (Fig. 1). At this amplitude, there are several interesting
 507 and important finite amplitude phenomena, including very large float (material) displacements given
 508 sufficient time. Nevertheless, a great deal of what we can see in a solution for $\eta(x, y, t)$ and $\mathbf{V}(x, y, t)$ can
 509 be attributed to linear wave dynamics and especially to the dispersion property of the waves supported
 510 by the linear shallow water system. (more on this below and in Part 3). The linear subset of the shallow
 511 water model results when $D(\)/Dt$ is replaced everywhere by $\partial(\)/\partial t$, and the variable layer thickness h
 512 is replaced by the constant initial thickness, H . In Cartesian components the linear shallow water model
 513 is

$$\begin{aligned}
 \frac{\partial h}{\partial t} &= -H\left(\frac{\partial u}{\partial x} + \frac{\partial v}{\partial y}\right), \\
 \frac{\partial u}{\partial t} &= -g'\frac{\partial h}{\partial x} + fv, \\
 \frac{\partial v}{\partial t} &= -g'\frac{\partial h}{\partial y} - fu.
 \end{aligned}
 \tag{30}$$

515 The stratification is represented in this one layer model by g' and H and assumed homogeneous.
 516 The stratification determines the phase speed of waves. The f in these equations is in general dependent

⁸Terms like $u \partial h/\partial x$ that are the product of two dependent variables are sometimes said to be 'bilinear' or 'semi-linear'. Model equations having such terms are nonlinear in the most important sense that a superposition of valid solutions does not yield a new valid solution. However, some solution methods are applicable to semi-linear systems, e.g., the method of characteristics, that are not applicable to more comprehensively nonlinear systems.

517 upon latitude (or north distance, y); the spatial variation of f determines the kinds of waves that are
 518 possible.

519 2.3 Boundary and initial conditions define the problem

520 The mass and momentum equations (16) and (17) could be used to model a wide range of phenomena.
 521 The definition of a specific, solvable problem follows from the specification of an initial condition on h
 522 and \mathbf{V} throughout the model domain, and the definition of boundary conditions along the edges of the
 523 domain.

524 The problems studied here are variants on the classical problem of geostrophic adjustment² and
 525 specifically, geostrophic adjustment of a mesoscale eddy-like feature at mid-latitude. The stratification
 526 is chosen to be typical of the subtropical main thermocline,

$$527 \quad H = 500 \text{ m and } \delta\rho = 2 \text{ kg m}^{-3}, \quad (31)$$

528 and the resulting gravity wave speed,

$$529 \quad C = \sqrt{g(\delta\rho/\rho_o)H} \approx 3.1 \text{ m s}^{-1},$$

530 is that of an internal or baroclinic gravity wave (Sec. 2.4.2). The initial condition is either a
 531 one-dimensional ridge with half-width L ,

$$532 \quad \eta(x, t = 0) = \eta_o \text{ if } |x| \leq L, \text{ or else } \eta(x, t = 0) = 0, \quad (32)$$

533 (here in Sec. 3) or a two-dimensional eddy with radius = L (in Sec. 4).⁹ The half-width and the
 534 amplitude of the initial interface displacement are chosen to be comparable to observed mid-latitude
 535 mesoscale eddies (Fig. 1),

$$536 \quad L = 100 \text{ km and } \eta_0 = 50 \text{ m}. \quad (33)$$

537 The initial velocity can be one of several forms, the default being a state of rest,

$$538 \quad \mathbf{V}(x, t = 0) = 0. \quad (34)$$

⁹The initial ridge given by Eqn. (32) has a very sharp edge, which in (numerical) practice is smoothed over a few horizontal grid points. Nevertheless, when released suddenly, this initial condition tends to produce energetic gravity waves that are not highly realistic of most natural phenomenon. Wind or tidal forcing acting on the ocean are by comparison rather slowly varying in time and space, and so less apt to produce energetic gravity waves. The initial condition may be easily changed to something smoother, and for that matter, the models may be readily configured to allow realistic wind or tidal forcing as in Part 3.

539 If the initial velocity and vorticity vanish, then the initial ridge has a potential vorticity $q = f/(H + \eta_o)$
 540 compared with f/H in the outlying fluid. This potential vorticity anomaly is preserved during
 541 geostrophic adjustment, the full import of which will become clear in Sec. 4.5.

542 The computational domain will be either one-dimensional, having a width of several thousand
 543 kilometers, where that is appropriate (Secs. 3 and 4, where f is presumed to be a constant), or
 544 two-dimensional and 4000 km on a side (Sec. 5). There is no attempt to compute the fluid state outside
 545 of the computational domain, and so something other than the momentum and continuity equations will
 546 have to be imposed on the boundaries.

547 The only energy in the initial state is associated with the initial eddy which is placed near the
 548 center of the model domain. It is then reasonable that waves will be radiated outward only, i.e., that
 549 nothing will come into the model domain from the outside. A plausible and generally effective
 550 representation of this one-way, outward transfer is made by imposing a radiation boundary condition
 551 along the boundaries:

$$552 \quad \frac{\partial \psi}{\partial t} = -U_{rad} \frac{\partial \psi}{\partial n}, \quad (35)$$

553 where ψ is thickness or a velocity component, n is the direction normal and outward from the boundary
 554 and U_{rad} is the appropriate velocity component normal to the boundary. This amounts to imposing a
 555 one-dimensional advection process normal to the boundary and at the speed U_{rad} , which is very
 556 important to the success of (35). The appropriate value of U_{rad} depends upon the dominant process
 557 local to the boundary, and that may change with time. Here, during the first 20 days of an experiment,
 558 U_{rad} is taken to be the gravity wave speed, $U_{rad} = C = \sqrt{g'H}$, the fastest wave speed in the shallow
 559 water system (Sec. 3.1). This serves well to usher along the gravity waves that first reach a distant
 560 boundary. But after that comes trouble ... very, very slowly ... in the form of low frequency Rossby
 561 waves (in Part 3).

562 2.4 Appendix to Sec. 2: Normal modes of a two layer model ocean

563 The shallow water model applied to a homogeneous (unstratified and so *barotropic*) ocean stands on its
 564 own. But if the shallow water model is applied to internal or *baroclinic* motions (defined below), then
 565 some discussion of the correspondence between observed and modelled layer thicknesses and phase
 566 speeds seems necessary.¹⁰ In that vein it is useful to examine briefly the wave properties of a simple two

¹⁰The terms barotropic and baroclinic describe the dependence of density upon pressure. A barotropic fluid is one in which the density can be written as a function of the pressure only, $\rho = \rho(P)$. This would hold always in a fluid that was homogeneous, for example, in the (single layer) shallow water model. It would also hold in a fluid that was density stratified, provided that the density surfaces and pressure surfaces were everywhere parallel. This would likely be true in a resting state, but not when motion causes vertical displacements of density surfaces that will often greatly exceed the associated

567 layer model. For this purpose rotation and nonlinearity may be ignored, and the motion presumed to be
 568 in one horizontal dimension only (x, t) . The stratification is represented by two homogeneous layers,
 569 Fig. (6), an upper layer 1, having an undisturbed thickness H_1 and density ρ_1 , and a lower layer, 2, with
 570 undisturbed thickness H_2 and slightly greater density, $\rho_2 = \rho_1 + \delta\rho$. If this was meant to represent the
 571 open ocean, then the interface between the layers would correspond with the middle of the main
 572 thermocline and typical values would be $H_1 = 500$ m, $H_2 = 3500$ m, $\rho_1 = 1030$ kg m⁻³ and
 573 $\rho_2 = \rho_1 + \delta\rho$ with $\delta\rho = 2$ kg m⁻³.

574 The interest here is in large scale, fairly slowly varying motions for which vertical accelerations are
 575 very, very gentle, $\ll g$, and the pressure is consequently hydrostatic, i.e., due to the weight of the fluid
 576 overhead. The bottom pressure is $P_b = g(\rho_1 h_1 + \rho_2 h_2)$, and the pressure within the layers varies as

$$577 \quad P_1(x, z, t) = g\rho_1(h_1(x, t) + h_2(x, t) - z) \quad \text{and} \quad P_2(x, z, t) = g\rho_1 h_1(x, t) + g\rho_2(h_2(x, t) - z),$$

578 where $h(x, t)$ is the space and time-varying layer thickness. The pressure gradient divided by the density
 579 is then in each layer,

$$580 \quad \frac{1}{\rho_1} \frac{\partial P_1}{\partial x} = g \left(\frac{\partial h_1}{\partial x} + \frac{\partial h_2}{\partial x} \right) \quad \text{and} \quad \frac{1}{\rho_2} \frac{\partial P_2}{\partial x} = g \frac{\rho_1}{\rho_2} \frac{\partial h_1}{\partial x} + g \frac{\partial h_2}{\partial x}. \quad (36)$$

581 With these results in hand, the momentum and continuity equations for the velocity and layer
 582 thicknesses are (anticipating a matrix format):

$$583 \quad \begin{aligned} \frac{\partial u_1}{\partial t} + g \frac{\partial h_1}{\partial x} + g \frac{\partial h_2}{\partial x} &= 0, \\ H_1 \frac{\partial u_1}{\partial x} + \frac{\partial h_1}{\partial t} &= 0, \\ g \frac{\rho_1}{\rho_2} \frac{\partial h_1}{\partial x} + \frac{\partial u_2}{\partial t} + g \frac{\partial h_2}{\partial x} &= 0, \\ H_2 \frac{\partial u_2}{\partial x} + \frac{\partial h_2}{\partial t} &= 0. \end{aligned} \quad (37)$$

584 Notice that the thickness of a given layer can vary only if there is divergence within that layer, and, that
 585 the pressure gradient has a dependence upon both layer thicknesses. Thus the pressure gradient couples
 586 the layers together.

displacement of pressure surfaces. In that case, the fluid would be described as baroclinic, meaning that density and pressure surfaces intersect, and so density varied with more than the pressure, i.e., with horizontal position and time at a given pressure. Thus, barotropic is a special case in which density surfaces are always parallel with pressure surfaces, while baroclinic is all else. The distinction is important in that the pressure gradient can (will) generate vertical shear in a baroclinic fluid, but not in a barotropic fluid. Thus a shallow water model will be realistic model of a barotropic fluid and flow. A shallow water solution will require some interpretation if, as here, it is meant to represent a baroclinic phenomenon, e.g., ocean mesoscale eddies.

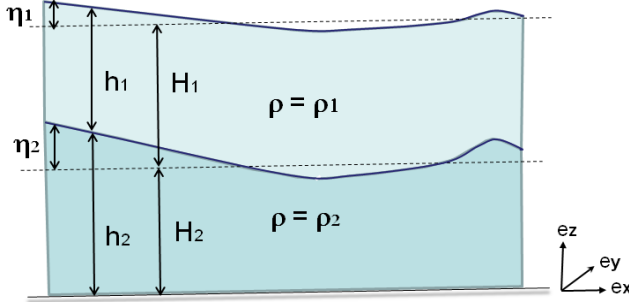


Figure 6: A two layer model appropriate to the stratified ocean. The dashed lines are level surfaces. The undisturbed layer thicknesses are H_1 and H_2 , and the actual thicknesses are h_1 and h_2 . The upper surfaces of the layers are displaced to $\eta_1 = h_1 + h_2 - (H_1 + H_2)$ and $\eta_2 = h_2 - H_2$. The pressure of the atmosphere above is presumed horizontally uniform and so negligible.

587 To find the wave properties of this system, presume that a wave may exist in both layers:
 588 $u_1(x, t) = U_1 \cos(kx - \omega t)$, $u_2(x, t) = U_2 \cos(kx - \omega t)$, $h_1(x, t) = H_1 + \Gamma_1 \cos(kx - \omega t)$ and
 589 $h_2(x, t) = H_2 + \Gamma_2 \cos(kx - \omega t)$. The U_1 , Γ_1 , U_2 , Γ_2 are constant but to this point unknown amplitudes.
 590 Notice that the wave frequency and wavenumber are the same in the two layers, which is implicit in 'a
 591 wave', and are also unknown. After substitution of this wave form, the governing equations (37) may be
 592 written in matrices as

$$593 \begin{pmatrix} -\omega & gk & 0 & gk \\ H_1 k & -\omega & 0 & 0 \\ 0 & gk \frac{\rho_1}{\rho_2} & -\omega & gk \\ 0 & 0 & H_2 k & -\omega \end{pmatrix} \begin{pmatrix} U_1 \\ \Gamma_1 \\ U_2 \\ \Gamma_2 \end{pmatrix} = 0.$$

The simplest and most insightful description of a multi-part, linear system such as this will often be in terms of the normal mode frequencies and structure, also called the eigenvalues and eigenvectors. The normal modes are independent of one another, and hence the governing equations written in terms of the normal modes will be decoupled, which is not the case with Eqns. (37) written in the layer-wise thickness and velocity. To find the frequencies of the normal modes it is necessary to solve the characteristic equation of the coefficient matrix (same as saying that the determinant must vanish), which is a fourth order polynomial in ω

$$\omega^4 - gk^2(H_1 + H_2)\omega^2 + g^2k^4H_1H_2\left(\frac{\rho_2 - \rho_1}{\rho_2}\right) = 0.$$

594 This characteristic equation is bi-quadratic (the cubic and linear terms vanish) and can be readily solved

595 as a quadratic equation for ω^2 ,

$$596 \quad \omega^2 = \frac{gk^2(H_1 + H_2)}{2} \pm \frac{\sqrt{g^2k^4(H_1 + H_2)^2 - 4g^2k^4H_1H_2\left(\frac{\rho_2 - \rho_1}{\rho_2}\right)}}{2}. \quad (38)$$

597 In the oceanic case in which $\frac{\rho_2 - \rho_1}{\rho_2} \ll 1$ this may be simplified by factoring the term under the square
598 root and then using the binomial theorem that $(1 + \varepsilon)^{1/2} \approx 1 + \varepsilon/2$ when $\varepsilon \ll 1$ as applies here,

$$599 \quad \omega^2 = \frac{gk^2(H_1 + H_2)}{2} \pm gk^2 \frac{(H_1 + H_2)}{2} \left(1 - 2 \frac{H_1H_2}{(H_1 + H_2)^2} \left(\frac{\rho_2 - \rho_1}{\rho_2} \right) \right). \quad (39)$$

600 2.4.1 Barotropic normal mode

601 The larger of the two roots of Eqn. (39) is the frequency squared of the external or *barotropic* mode,

$$602 \quad \omega_{btr}^2 = gk^2(H_1 + H_2) - gk^2 \frac{H_1H_2}{(H_1 + H_2)} \left(\frac{\rho_2 - \rho_1}{\rho_2} \right). \quad (40)$$

603 Since the trailing factor involving the density difference is very, very small, ≈ 0.002 , an excellent
604 approximation of this frequency is

$$605 \quad \omega_{btr} \approx \pm k \sqrt{g(H_1 + H_2)}. \quad (41)$$

606 If the intent is to reproduce this dispersion relationship within a shallow water model, then the
607 single-layer equivalent gravity and layer thickness are simply

$$608 \quad g_e = g, \quad \text{and} \quad H_e = H_1 + H_2, \quad (42)$$

609 which might have been guessed without help from a two layer model. This is the barotropic mode. The
610 same kind of result is slightly less obvious for the baroclinic mode coming next.

611 By putting the appropriate frequency (41) back into the governing equations (37) we can solve for
612 the ratio of the amplitude of the layer thicknesses changes,

$$613 \quad \frac{\Gamma_1}{\Gamma_2} = \frac{\rho_2}{2\rho_1} \left((H_1 + (H_1^2 + H_2^2 - 2H_1H_2 + 4H_1H_2\frac{\rho_1}{\rho_2})^{1/2})/H_2 - 1 \right). \quad (43)$$

614 Noting that ρ_1/ρ_2 is very close to 1, then as a very good approximation,

$$615 \quad \frac{\Gamma_1}{\Gamma_2} \approx \frac{H_1}{H_2}. \quad (44)$$

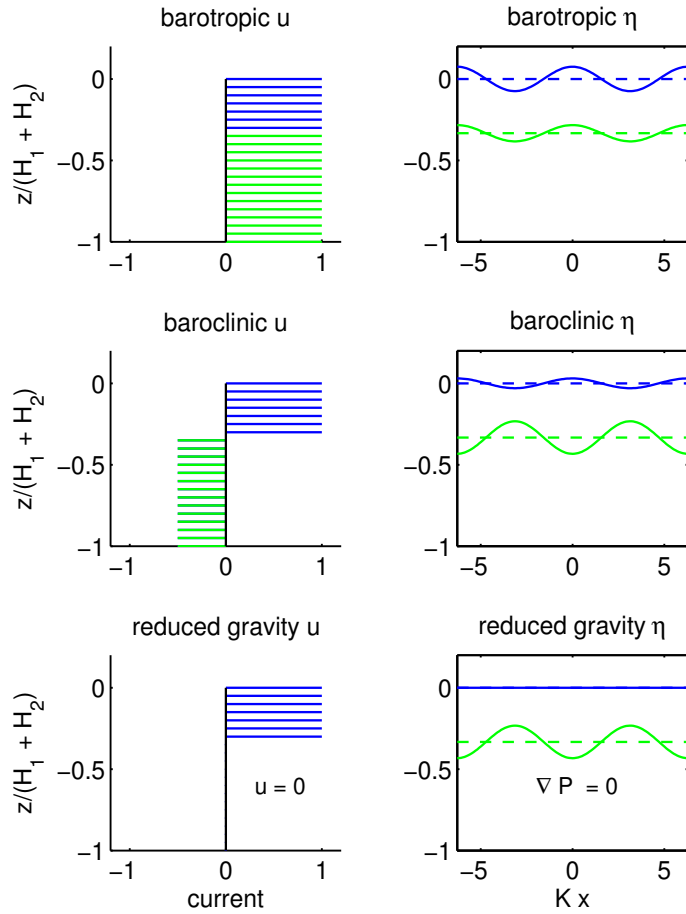


Figure 7: Normal modes of a two-layer ocean. **(upper)** The barotropic normal mode; current profile (upper left, arbitrary amplitude) and the sea surface and interface displacements (upper right, blue and green lines). **(middle)** The baroclinic normal mode. The currents and the sea surface and interface displacements have a self-consistent structure, but the thicknesses, $H_1 = 500$ m and $H_2 = 1000$ m, and the density difference, $\delta\rho = 300 \text{ kg m}^{-3}$, were chosen to make this structure legible rather than realistic of the ocean thermocline. **(lower)** The reduced gravity approximation of the baroclinic mode uses only the density interface to compute the pressure gradient in the upper layer on the assumption that the lower layer currents and pressure gradient vanish. This would not be a good approximation for the stratification shown in this figure because H_1/H_2 is not $\ll 1$.

616 In this linear model the amplitude of either Γ_1 or Γ_2 is arbitrary, but the ratio Γ_1/Γ_2 is determined by
 617 the dynamics. Eqn. (44) indicates that the layer thicknesses oscillate in phase and with an amplitude
 618 that is proportional to the undisturbed layer thickness. For some purposes it is helpful to know the
 619 displacement of the upper surfaces of the layers; the sea surface, sometimes called the free surface, is
 620 displaced from its resting (level) height by

$$621 \quad \eta_1 = (h_1 + h_2) - (H_1 + H_2),$$

622 and the density interface between the layers by

$$623 \quad \eta_2 = h_2 - H_2.$$

624 In the barotropic mode, the amplitude of the vertical displacement of the free surface compared to the
 625 displacement of the interface is then, using Eqn. (44),

$$626 \quad \frac{\Gamma_1 + \Gamma_2}{\Gamma_2} = \frac{H_1 + H_2}{H_2} \approx 1.14, \quad (45)$$

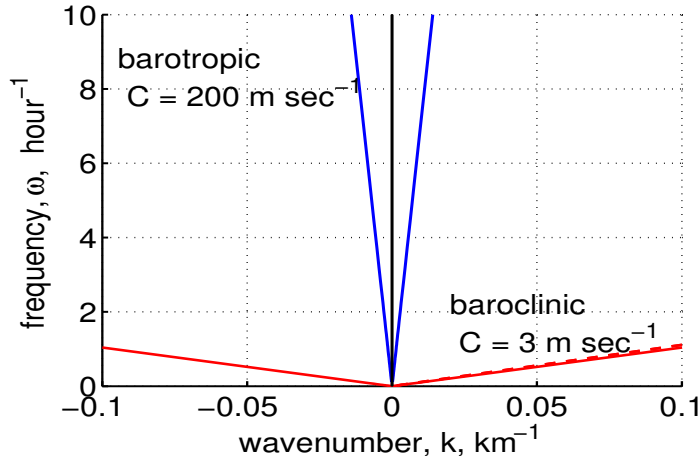


Figure 8: The dispersion relation for gravity waves of a two layer, nonrotating model of a stratified ocean. The solid lines are the full dispersion relation, and the dashed red line is an approximation discussed in the main text. At a common wavenumber, the barotropic and baroclinic modes have vastly different frequencies and phase speeds.

627 for our nominal, open ocean stratification. The vertical displacement is thus a maximum at the sea
 628 surface and decreases linearly to zero at the bottom (Fig. 7, upper). The displacements $\eta_1(x, t)$ and
 629 $\eta_2(x, t)$ have a $\cos(kx - \omega t)$ time- and space-dependence that is common to both layers, which is what
 630 distinguishes a mode from an arbitrary motion. The pressure gradient is due almost entirely to the
 631 displacement of the free surface, and the currents are the essentially the same in the two layers (uniform
 632 with depth). The density interface η_2 moves up and down exactly as does the pressure at that level, and
 633 thus the density could be written as a function of the pressure in the initial state and during the
 634 subsequent motion. This kind of wave motion in which $\rho = \rho(P)$ everywhere in the fluid is, as here,
 635 termed barotropic.

636 The phase speed of a barotropic wave for a nominal, open ocean depth $H_1 + H_2 = 4000$ m is very
 637 fast,

$$638 \quad C_{btr} = \frac{\omega_{btr}}{k} = \sqrt{g(H_1 + H_2)} \approx 200 \text{ m sec}^{-1} \approx 680 \text{ km hour}^{-1},$$

639 or comparable to that of a jet transport. High frequency (5 to 20 min period) barotropic waves of this
 640 kind (in some circumstances called *tsunamis*, Japanese for harbor wave) are the primary oceanic
 641 response to a rapid vertical displacement of the sea floor (a few meters in a few minutes over a large
 642 horizontal scale). Because the fluid velocity associated with open ocean tsunami waves is comparatively
 643 gentle, a few centimeters per second, these waves undergo very little dissipation, and, aside from
 644 two-dimensional spreading, may arrive on a distant shore with a significant amplitude. Lower frequency
 645 barotropic waves (periods 1/2 to 1 day) are the principal components of the open ocean, astronomical
 646 tides. These near-daily frequency waves gravity waves are modified substantially by Earth's rotation
 647 and are often called inertia-gravity waves (Sec. 4, also called Poincare waves).¹¹

¹¹An excellent resource for tsunami waves is <http://www.tsunami.noaa.gov/> A classic paper on open ocean tides is by <http://articles.adsabs.harvard.edu//full/1944MNRAS.104..244P/0000254.000.html>

648 **2.4.2 Baroclinic normal mode**649 The smaller of the two roots of Eqn. (39) is labeled the internal or *baroclinic* normal mode, and

650
$$\omega_{bcl} = \pm k \sqrt{g \frac{H_1 H_2}{(H_1 + H_2)} \left(\frac{\rho_2 - \rho_1}{\rho_2} \right)}. \quad (46)$$

Baroclinic gravity waves have a much lower frequency and phase speed than does a barotropic wave of the same wavelength,

$$\frac{\omega_{bcl}}{\omega_{btr}} = \frac{C_{bcl}}{C_{btr}} \approx \sqrt{\frac{g' H_1 H_2}{g (H_1 + H_2)^2}} \approx \frac{1}{70},$$

651 mainly because the reduced gravity, $g' = g(\rho_2 - \rho_1)/\rho_2 = g(2/1000)$, is very much less than the full
652 gravity, g . If the intent is to model the baroclinic dispersion relation using a shallow water model, then

653
$$g_e = g' \quad \text{and} \quad H_e = \frac{H_1 H_2}{(H_1 + H_2)} \quad (47)$$

will give an appropriate phase speed.¹² It is usually the case that H_2 exceeds H_1 by a factor of 5 - 10, and as a fair approximation, $H_e \approx H_1$. The baroclinic, long gravity wave phase speed is then, for the nominal stratification,

$$C_{bcl} = \frac{\omega_{bcl}}{k} = \sqrt{g' H_1} \approx 3.1 \text{ m sec}^{-1} \approx 270 \text{ km day}^{-1},$$

654 the red line of Fig. (8).

655 The ratio of layer thicknesses in the baroclinic mode is

656
$$\frac{\Gamma_1}{\Gamma_2} = \frac{\rho_2}{2\rho_1} \left((H_1 - (H_1^2 + H_2^2 - 2H_1 H_2 + 4H_1 H_2 \frac{\rho_1}{\rho_2})^{1/2}) / H_2 - 1 \right). \quad (48)$$

657 Making the same approximation noted earlier for the barotropic mode,

658
$$\frac{\Gamma_1}{\Gamma_2} \approx -\frac{\rho_2}{\rho_1} \approx -1, \quad (49)$$

659 and hence the layer thicknesses oscillate out of phase, and with nearly equal amplitude (Fig. 7, middle).

660 There is a small but very important displacement of the free surface,

661
$$\frac{\Gamma_1 + \Gamma_2}{\Gamma_2} \approx -\frac{\rho_2 - \rho_1}{\rho_1} = -0.0017,$$

¹²Most authors define the equivalent depth from phase speed only, i.e., $H_e = C_{bcl}^2/g$ with g the full gravity. With that definition, the baroclinic $H_e \approx 1$ m (!). In other words, the baroclinic gravity wave mode has the phase speed of a 1 m thick, homogeneous (barotropic) layer. In a linear shallow water model and problem, the phase speed is all that matters and this can be a useful definition. However, if the shallow water model includes finite amplitude effects and is intended to simulate realistic amplitudes, then the actual layer thickness is relevant, and the equivalent values of Eqn. (47) seem more apt.

662 for the given stratification. An interface (thermocline) displacement of 50 m will thus be accompanied
 663 by a free surface displacement of about $50 * (\delta\rho/\rho_o) \approx 10$ cm, which is readily detectable to
 664 satellite-based, altimetric methods, as in Fig. (2). The currents in the upper and lower layers are exactly
 665 out of phase, and their ratio is such that the net transport vanishes.

666 2.4.3 Reduced gravity approximation of the baroclinic normal mode

667 The transport (depth integrated velocity) of the baroclinic normal mode $= u_1 H_1 + u_2 H_2 = 0$. Thus the
 668 upper and lower layer currents are in the ratio $u_1/u_2 = -H_2/H_1$. In the limit that $H_1/H_2 \rightarrow 0$, the lower
 669 layer current and pressure gradient are much, much less than in the upper layer. In that case, an
 670 approximation of Eqn. (36) is that

$$671 \quad \frac{\partial h_2}{\partial x} = -\frac{\rho_1}{\rho_2} \frac{\partial h_1}{\partial x},$$

672 which may be used to eliminate the h_2 term from the upper layer pressure gradient,

$$673 \quad \frac{\partial P_1}{\partial x} = g \left(\frac{\rho_2 - \rho_1}{\rho_2} \right) \frac{\partial h_1}{\partial x} = g' \frac{\partial h_1}{\partial x}.$$

674 The density interface can thus be used as a proxy for the sea surface insofar as the pressure gradient in
 675 the upper layer is concerned, provided that the full gravity that multiplies the sea surface slope is
 676 replaced by the much smaller reduced gravity, g' , multiplying the much greater slope of the density
 677 interface. In that way all reference to the lower layer may be eliminated from the upper layer equations.
 678 This is sometimes referred to as a one and a half layer model, where the half refers to the deep, resting
 679 lower layer, and it is also called the reduced gravity approximation, (Fig. 7, lower). This is an
 680 appropriate interpretation of the shallow water model when applied to a simulation of baroclinic,
 681 mesoscale eddies which are mainly upper ocean (layer one) phenomena, and plausible for modelling
 682 some aspects of the wind-driven circulation of subtropical gyres (Fig. 9 and more in Part 4). The
 683 reduced gravity approximation may also be used in a multi-layered model, so long as it is appropriate to
 684 approximate the deep flow and pressure gradient as vanishing.

685 2.5 Problems

686 (1) What is the interpretation of $d/dt = 0$ in a Lagrangian system? How about $\partial/\partial t = 0$ and $D/Dt = 0$
 687 in an Eulerian system? The material derivative and some aspects of advection are discussed in greater
 688 detail in 'Lagrangian and Eulerian representations...'. Price, James F., 12.808 Supplemental Material,
 689 Topics in Fluid Dynamics: Dimensional Analysis, the Coriolis Force, and Lagrangian and Eulerian
 690 Representations, <http://ocw.mit.edu/ans7870/resources/price/index.htm>

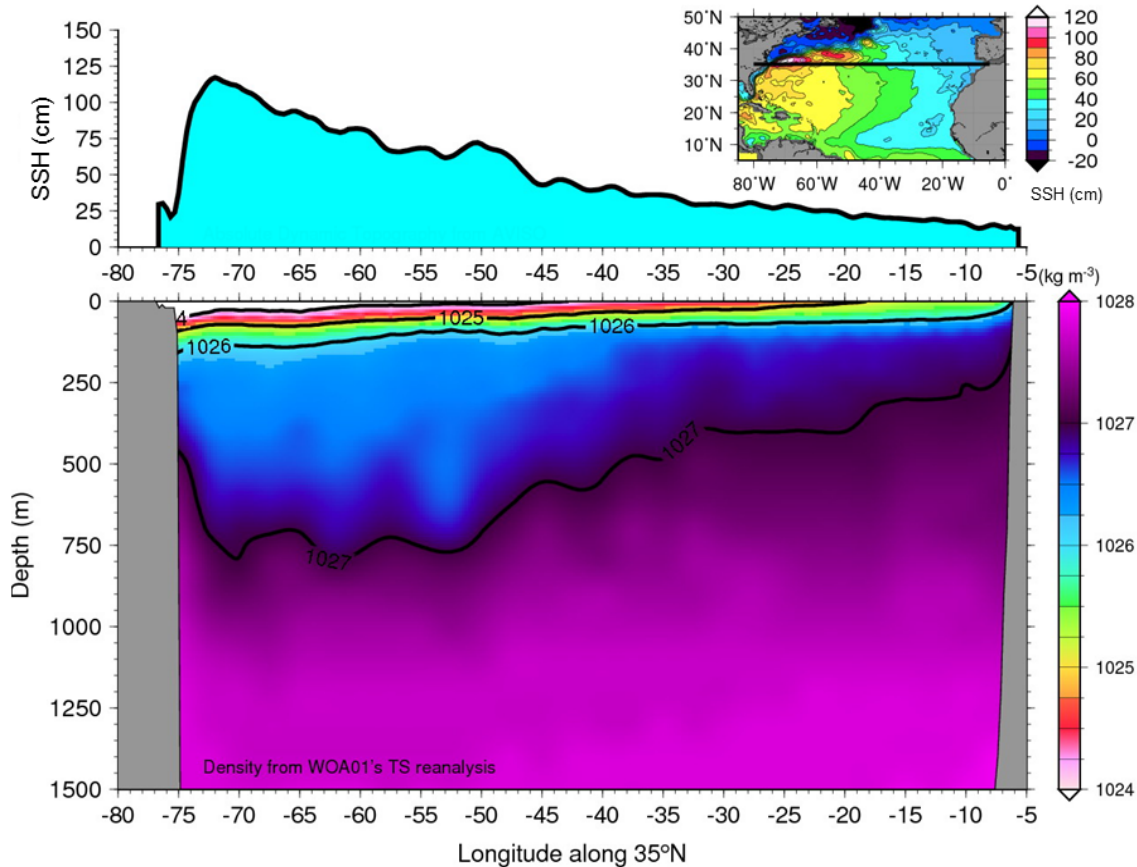


Figure 9: A cross section of the North Atlantic subtropical thermocline, sliced east-west along 35°N , and viewed looking toward the north. The upper panel is SSH as in Fig.1, but here the monthly average for September over about twenty years of measurement. The lower panel is the long-term, September average of density along 35°N from the World Ocean Atlas 2001 (http://www.nodc.noaa.gov/OC5/WOA01/pr_woa01.html). The tilt of the thermocline mirrors the tilt of the sea surface so that high SSH corresponds to a thick, warm upper layer. A result is that the pressure gradient and geostrophic velocity are comparatively small in the abyssal ocean, roughly 1500 - 2500 m depth, suggestive of a reduced gravity approximation (Section 2.4.3). Not shown in this figure are bottom-trapped density currents found at depths in excess of about 3000 m that make up the lower limb of the meridional overturning circulation. This figure was kindly provided by Iam-Fei Pun of WHOI.

691 (2) If phase speed and group speed are not already familiar to you, then the very brief discussion of
 692 Sec. 2.2.1 will probably not suffice. An excellent primary reference is Chapters 1 and 2 of Pedlosky's
 693 'Waves in the Ocean and Atmosphere' (footnote 3). For a quick refresher, you might take a look at the
 694 script `twowaves.m` (Sec. 6.3), which allows you to define an arbitrary dispersion relationship between
 695 two waves that are then superimposed. The envelope of the superposition, and thus a wave form or
 696 pulse, propagates at the group speed, $C_g = \delta\omega/\delta k$, where δ is the difference between the two waves.

697 (3) You will feel much more at ease with the important energy and potential vorticity conservation
 698 laws if you will take the time to derive them yourself. There are no special techniques or
 699 approximations required, though the full shallow water equations entail a fair degree of manipulation. It
 700 will be helpful to start with the linear shallow water equations (see the next section) and then add just
 701 one of the advection terms, say $u\partial h/\partial x$. And if you need to peek:
 702 www.eos.ubc.ca/courses/eosc477/content/pv_deriv.pdf Performing this derivation does not aid
 703 applications, but it does help answer two important questions. 1) Does the linear shallow water system
 704 yield a self-consistent energy and vorticity balance? 2) Does the q conservation law include all of the
 705 phenomena of the shallow water system? How about energy conservation? (This second question will
 706 be answered in Sec. 3.1.)

707 (4) Some q -conservation problems for you: 1) A right cylinder having a radius r and height h has a
 708 moment of inertia $I = Mr^2/2$ where M is the mass of the cylinder. The angular momentum due to
 709 rotation at a rate ω about the central axis is $L = I\omega$. Show that conservation of angular momentum
 710 under changes of h and r that are mass (volume) conserving can be summarized with a vorticity
 711 conservation law like Eqn. (29). 2) Because $f \gg \xi$, generally, a change in thickness of 10% is often
 712 highly significant for the relative vorticity, as is a change in latitude of only a few degrees. Assume that
 713 a fluid column having a radius of 50 km and a thickness of 700 m is moved from 40°N to 25°N and that
 714 it conserves q . If all of the change in f is accounted by changes in ξ (no thickness change), estimate the
 715 magnitude of the resulting current. Now suppose that the change in f is accommodated entirely by a
 716 change in thickness.....how much?

717 (5) The algebra required for a three layer model is a bit tedious and is a good application for symbolic
 718 mathematics; see `twolayer_eig.m` linked in Sec. 6.3.

719 (6) Some modal questions for you: 1) Any arbitrary configuration of layer thicknesses may be
 720 decomposed into the normal modes. What would you infer is the two layer model composition of the
 721 offhand sketch of layer thicknesses in Fig. (6)? 2) In place of two active layers, suppose three layers of
 722 equal thickness. What would you guess for the modal structure of η ? Check your answer against the
 723 (numerical) eigenvectors of `twolayer_eig.m` (Sec. 6.3). 3) The reduced gravity approximation is
 724 counterintuitive in that the density interface displacement is used to compute the hydrostatic pressure
 725 anomaly in the layer *above* the density interface. Rather than try to explain that while developing the
 726 shallow water model in Sec. 2.1, this valuable and sensible approximation (or interpretation) was
 727 deferred to this appendix. The essential, physical connection between pressure and mass or thickness
 728 anomaly is that a comparatively thick upper layer is a region of high pressure anomaly, as in Fig. (9).
 729 What do you think would happen if, due to a sign error in the code of a numerical model (we all make
 730 them) this relationship was reversed?

731 3 Gravitational adjustment

732 The sequence of experiments described here and in Part 3 differ mainly in the way that Earth's shape
 733 and rotation are represented. Of course, we know that the Earth is approximately spherical and that the
 734 Coriolis parameter varies significantly with latitude. Nevertheless, in the first experiments described
 735 here in Sec. 3, the model domain is presumed to be flat and not rotating, i.e.,

$$736 \quad f = 0,$$

737 and there is no Coriolis force. In that case the shallow water model supports pure gravity waves only.
 738 Then, in Sections 4 and 5, the Earth will be approximated as rotating but flat, i.e.,

$$739 \quad f = \text{constant},$$

740 in which case there are gravity waves, inertial oscillations and geostrophic motions all at once. With an
 741 understanding of those experiments in hand, we will then be ready in Part 3 for the realistic case,
 742 spatially varying

$$743 \quad f(\text{latitude}),$$

744 first a mid-latitude case and then an equatorial case. These latter two experiments will include all of the
 745 phenomena that arise here, plus a low frequency wave motion called a planetary or Rossby wave.

746 3.1 Just gravity waves

747 The experiment starts at $t = 0$ when the thickness anomaly of dense water is released. Within the first
 748 tens of minutes the ridge begins to slump under the force of gravity, releasing potential energy and
 749 generating currents (kinetic energy). In this experiment, the motions take the form of two equal,
 750 outgoing solitary 'wave pulses' of amplitude $\eta_o/2$ and width $2L$. These pulses move at a steady speed
 751 that is very close to the (baroclinic) gravity wave speed, $C = \sqrt{g'H}$, and hence they run off of the model
 752 domain in just a few days. Other than these two discrete wave pulses, there is nothing. If you (like the
 753 author) had expected the response to look something like the waves excited on the surface of a pond by
 754 an errant golf ball, or tsunami waves generated on the surface of the ocean by a moving sea floor, then
 755 this solution will seem strange indeed. This raises a string of questions, some that should arise in any
 756 numerical study, and others that are specific to this case. In the first place, how can we know that this
 757 numerical solution is faithful to the model equations? ¹³ And then, these pulses look nothing like
 758 elementary gravity waves and so is it appropriate to call them 'wave' pulses?

¹³Looking at the plot of a numerical solution is a little bit like looking at Saturn through a new, homemade telescope (Fig. 11, Part 1). Barring catastrophic errors, the largest eddies and the rings will be obvious and unmistakable. However, at

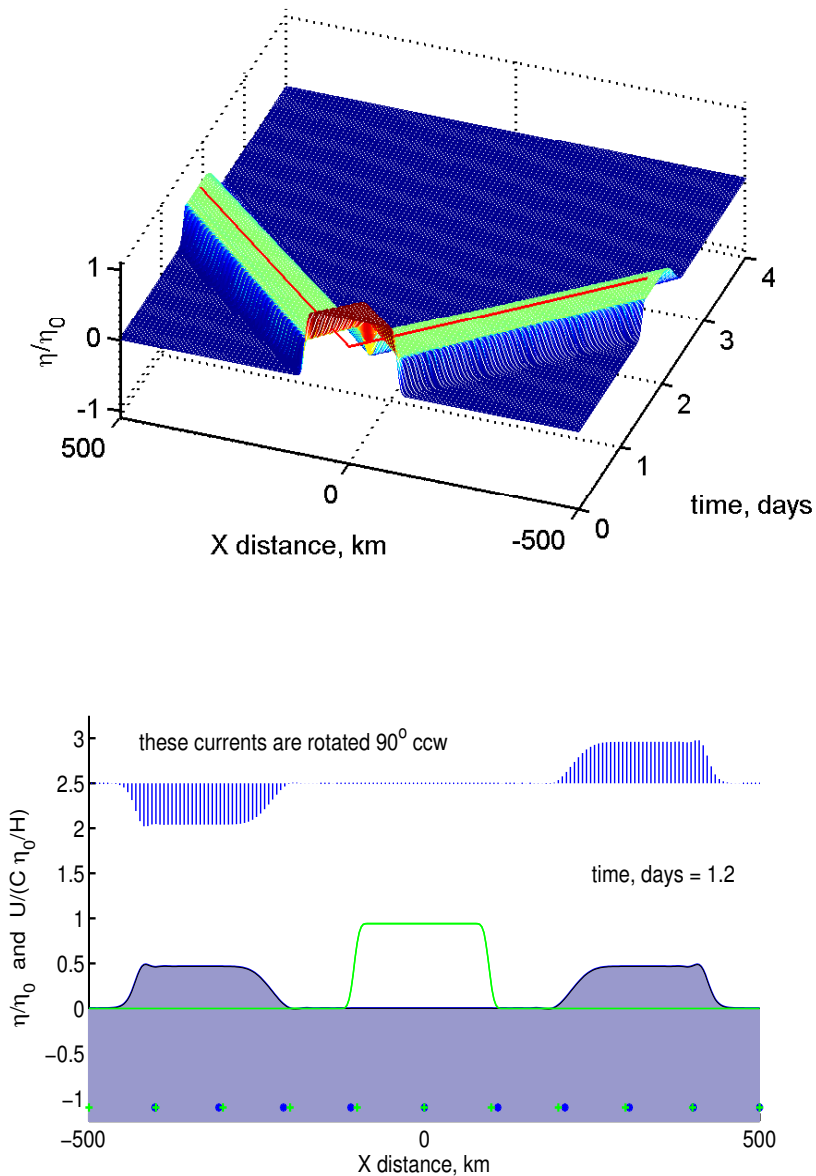


Figure 10: An experiment in gravitational adjustment (no rotation) solved by the numerical model `geoadj_1d.m` (Sec. 6.3). **(upper)** The nondimensional (scaled) thickness anomaly, $\eta(x,t)/\eta_0$, following the release of a rectangular ridge that had an initial amplitude $\eta_0 = 50\text{m}$. The thin red lines have a slope given by the gravity wave speed, $C = \sqrt{g'H} = 3.1 \text{ m s}^{-1}$ in this experiment. This solution was computed by the numerical model, `geoadj_1d.m` (Sec. 6.3). **(lower)** A snapshot of the solution at $t = 1.2$ days. The green line shows the initial thickness anomaly. The current, which is shown by the array of vectors plotted above, is in the x-direction only and has been rotated 90° counterclockwise to be made visible here. The current is scaled with $C\eta_0/H$ ($= 0.3 \text{ m s}^{-1}$ for the case $\eta_0 = 50 \text{ m}$). The blue dots and green crosses at depth $= -1.1$ show the present positions and the initial positions of floats. An animation of the lower panel is at: www.who.edu/jpweb/ga1-lat0.flv

759 3.2 An exact solution of the linear, one-dimensional wave equation

760 There is a well-known, exact analytic solution for the initial value problem of the linear
 761 one-dimensional wave equation that can serve as a very useful reference for some aspects of this
 762 numerical solution. The wave equation of the linear, nonrotating shallow water system, Eqns. (30) with
 763 $f = 0$ and $v = 0$) is readily found by eliminating u in favor of η (recall that $\eta = H + h$ with H a constant
 764 and so $\partial h/\partial t = \partial \eta/\partial t$),

$$765 \quad \frac{\partial^2 \eta}{\partial t^2} = g'H \frac{\partial^2 \eta}{\partial x^2}. \quad (50)$$

766 Given that the initial data is

$$767 \quad \eta(x, t = 0) = \eta_o(x), \quad (51)$$

768 then the d'Alembert solution

$$769 \quad \eta(x, t) = \frac{1}{2} \eta_o(kx - \omega t) + \frac{1}{2} \eta_o(kx + \omega t), \quad (52)$$

770 solves (50) and (51) provided that

$$771 \quad \omega = k \sqrt{g'H}. \quad (53)$$

772 The relationship $\omega(k)$ given by Eqn. (53) is called the dispersion relation, and is the crucial and
 773 distinguishing property of a wave system. This is a particularly simple dispersion relation, $\omega(k)$ being a
 774 straight line with slope $\sqrt{g'H}$, Fig. (8). Waves of all wavenumber thus have the same phase speed,

$$775 \quad \boxed{C_p = \frac{\omega}{k} = \sqrt{g'H} = C} \quad (54)$$

776 and the same group speed,

$$777 \quad \boxed{C_g = \frac{\partial \omega}{\partial k} = \sqrt{g'H} = C} \quad (55)$$

778 Because all of the waves in this system (that is to say, waves of all wavenumbers) have the same phase
 779 speed, this system (shallow water, linear, nonrotating) is said to be nondispersive. As a consequence,
 780 the initial shape, $\eta_o(x)$, is retained in the propagating wave pulses. Examples of dispersive wave
 781 systems arise in later problems. Notice that the phase and group speed in this linear model are
 782 dependent upon the stratification g' and H only, and are independent of the amplitude of the motion.

some level of detail an active skepticism is healthy, even essential to avoid over-interpretation or outright error. For example, would you notice that Saturn is somewhat flattened if you didn't anticipate it? How could you discern genuine flatness from an optical distortion? One way would be to observe other, better-known phenomenon, e.g., the Moon, to calibrate the instrument's performance and extrapolate from there. Something like that can be done for numerical solutions by verifying that they follow adequately (not perfectly) the conservation laws for energy and potential vorticity, among others, and that they reproduce known solutions well enough.

783 Gravity waves are the only possible nontrivial motion in this system. There is nothing that picks
 784 out a favored direction, and hence it is isotropic (from Greek *iso* + *tropos*, equal in all directions). Thus
 785 by symmetry half of the initial ridge propagates in one direction, and half goes the other.

786 The current that accompanies the wave pulses is in the direction of the pulse propagation, i.e.,
 787 toward positive x within the right-traveling pulse. The velocity and the pressure gradient within the
 788 pulses is thus colinear (parallel or anti-parallel), a relationship often termed longitudinal in this context,
 789 and that is characteristic of pure gravity wave motion. On the other hand, geostrophic motion is
 790 transverse insofar as the velocity and the pressure gradient are approximately normal to one another
 791 (Part 1, Sec. 5 and other examples coming soon). The observed velocity/pressure gradient relationship
 792 thus provides a useful qualitative clue to dynamics at the level of the momentum balance.

793 Perhaps the two most important points are that 1) comparison with the exact d'Alembert solution
 794 shows that the numerical solution of Fig. (10) is qualitatively correct (more details below), and 2) the
 795 isolated pulses seen in the numerical solution are gravity waves in all respects save their appearance.
 796 Their structure is that of the initial condition and is retained because of the nondispersive property of
 797 shallow water (nonrotating) gravity waves combined with the one-dimensional geometry of this specific
 798 problem.

799 3.3 The choice of scales

800 There is usually more than one way to plot a model solution (Fig. 10). It is highly desirable to use
 801 coordinates that will allow for use by the broadest possible audience. This generally requires the use of
 802 nondimensional coordinates, i.e., that independent variables, distance, time, etc. be reported in units
 803 that are intrinsic (natural) to the model system rather than in meters or seconds. In that respect, a
 804 curious feature of the linear, nonrotating shallow water model, Eq. (50), is that the gravity wave speed,
 805 $C = \sqrt{g'H}$, is the only intrinsic scale; there is no intrinsic horizontal length scale or time scale, as there
 806 will be when rotation is included in Sec. 3.1. Dimensional scales that are convenient for the specific
 807 initial condition, kilometers for horizontal distance and days for time, were therefore chosen for Fig.
 808 (10) and will be retained in all later plots to facilitate comparison with this first experiment.

809 The scales for the dependent variables, η and u , were chosen with the goal that the scaled
 810 (nondimensional) variables should be independent of the initial amplitude, η_0 , in the limit of small
 811 amplitude. The obvious scale for the thickness anomaly is η_0 , the initial value. Thus the thickness
 812 anomaly is plotted as η/η_0 . (To preserve the important sign of η_0 it is necessary to use the absolute
 813 value, $\eta/|\eta_0|$, though the plot legends do not show this.) The appropriate scale for the fluid speed is
 814 less obvious. The gravity wave speed $C = \sqrt{g'H}$ seems a promising candidate at first. However, C
 815 depends only upon the fluid properties and is independent of the amplitude, here η_0 , while the fluid

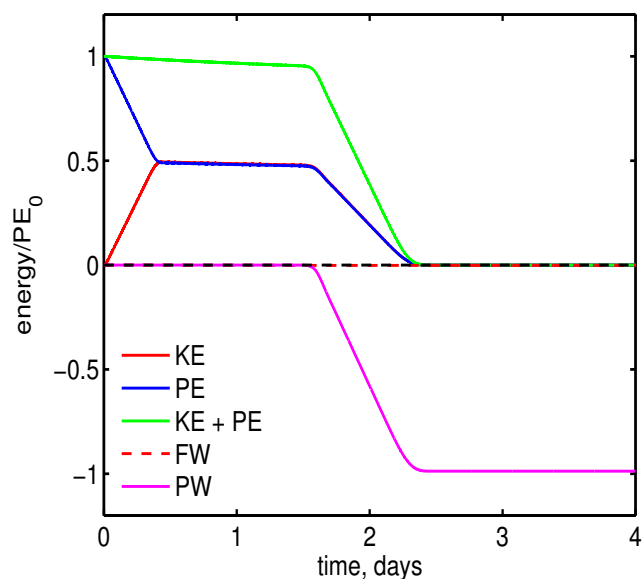


Figure 11: The energy balance for the gravitational adjustment problem (no rotation, Sec. 3.1) evaluated over a control volume $-500 \leq x \leq 500$ km. Energy is nondimensionalized with the initial potential energy, PE_0 , and time is in days. The first four curves shown here have the same meaning as the curves with the same name (and color) in the parcel on a slope problem of Part 1, Sec. 5. Frictional work (FW) is vanishingly small since the frictional parameter r was effectively zero in this experiment.

816 speed should increase roughly linearly with η_o . Hence, C alone is evidently not an appropriate scale for
 817 the fluid speed. As a guess let's try instead $C\eta_o/H$, i.e., plot $u/(C\eta_o/H)$ (Fig. 10). Note that the current
 818 amplitude is about 0.5 in these nondimensional units. If this is indeed an appropriate scaling, then the
 819 nondimensional (or normalized) fluid speed should remain about 0.5 when η_o is varied within a small
 820 amplitude regime. At a large enough amplitude, the nondimensional speed will depart from this linear
 821 scale, which can be interpreted as a finite amplitude effect.

822 3.4 Energy and potential vorticity balances

823 The energy balance (Sec. 2.3.2) was evaluated over a domain $-500 \leq x \leq 500$ km (Fig. 11). Several
 824 features of this energy balance are in common with the parcel on a slope (Part 1, Sec. 5.3). First, the
 825 only source of energy is the potential energy, PE, stored in the initial ridge, as is true in all of the
 826 geostrophic adjustment problems that follow. Second, after the ridge is released and begins to slump,
 827 the decrease of PE is accompanied by a closely comparable increase of kinetic energy, KE. Thus the
 828 total energy, KE + PE, is approximately conserved in this ideal shallow water model, aside from small
 829 losses (a few percent per week) due to numerical viscosity and to a small but numerically necessary
 830 horizontal diffusion (discussed below).

831 Other aspects of this energy balance are quite different from that of the single parcel experiment.
 832 Notice that once the outward-going wave pulses are fully separated, $t \geq 2L/C = 0.8$ days, the kinetic
 833 energy and potential energy are thereafter equal. This kind of energy equipartition is a characteristic of

834 (nonrotating) linear gravity wave motion and so provides a useful check on the numerical solution in the
 835 much more common case that an exact analytic solution is not available. A second difference is the
 836 domain over which the energy balance was diagnosed. There was no choice about where to evaluate the
 837 energy balance for a single parcel; of course the balance was computed for the moving parcel. In fluid
 838 dynamics parlance that would likely be called a Lagrangian (material-following) balance. Given the
 839 present fluid model, there are a number of other ways that an energy balance could be evaluated. The
 840 balance could follow a wave pulse, or it could follow any specific fluid column. Here, the energy
 841 balance is evaluated over a fixed control volume, which is oftentimes called an Eulerian balance. As
 842 one consequence, energy could leave the control volume through the sides beginning at $t \approx 1.6$ days
 843 when the wave pulses reach the edges of the control volume. This energy flux is accounted by the
 844 pressure work term of Eqn (25).

845 Potential vorticity is interesting in quite a different way — there isn't any! There is no planetary
 846 vorticity since $f = 0$, there is no relative vorticity in the initial condition since the ridge begins at rest,
 847 and there is no vorticity produced by the subsequent gravity wave processes because the pressure
 848 gradient in a shallow water model has zero curl.¹⁴ Potential vorticity analysis is often invaluable for the
 849 analysis of low frequency phenomenon (next sections), but here is a reminder that potential vorticity,
 850 and vorticity generally, is blind to shallow water gravity waves.

851 3.5 Finer details of the solution; finite amplitude effects

852 On first seeing this solution the question came up — in what ways and to what degree can we trust this
 853 numerical solution? If we were attempting to make a realistic simulation of an observed, physical
 854 phenomenon (we aren't) then we would have to consider the assumptions made in formulating the
 855 shallow water model. But here the issue is much narrower how can we test that the plots in front of
 856 us represent an acceptably accurate solution to the problem posed? Comparison of the numerical
 857 solution with the exact D'Alembert solution suggests that wave propagation aspects are simulated
 858 reasonably well in the sense that the pulses move at nearly the phase speed C , and without significant
 859 dispersion, as they should in a small amplitude limit. Energy is also balanced fairly closely, though
 860 there is an unaccounted loss of a few percent in the first week. This implies that the amplitude generally
 861 must be slightly low as well.

862 A close look reveals two other, small but systematic differences between the numerical solution
 863 and the exact, linear d'Alembert solution insofar as the numerical wave pulses do not retain the exact

¹⁴In a shallow water model the fluid density is presumed constant in space and in time. If instead the density varies in space, then the pressure gradient divided by the variable density may have a curl, often called a solenoidal term. This term will produce vorticity having a component normal to the plane of the pressure and density gradients. This baroclinic process can be important in a more general three-dimensional fluid, but can not arise here.

864 shape of the initial ridge. First, the numerical $\eta(x, t)$ shows a small scale spatial oscillation (wavelength
 865 several times the numerical grid interval) that is characteristic of a finite-differencing error.¹⁵ A second
 866 and more interesting difference is that the leading edge of a numerical wave pulse is steepened slightly,
 867 while the trailing edge is elongated or rarefied. This appears to be a genuine, finite amplitude effect due
 868 to nonlinear processes — horizontal advection and large variations in layer thickness — that are present
 869 in the nonlinear numerical model and solution, but not in the linear D'Alembert solution.

870 It is very useful to be able to make an *a priori* (before the event) estimate of the nonlinear terms
 871 and so to form a hypothesis regarding how finite amplitude effects may vary with the amplitude, η_o . For
 872 a longitudinal wave in which the wave and fluid velocity are colinear,
 873 $u \propto u_o \cos(kx - \omega t)$, $h \propto h_o \cos(kx - \omega t + \phi)$, the ratio of the nonlinear thickness advection term to the
 874 linear local time rate of change may be estimated as

$$875 \frac{\text{nonlinear}}{\text{linear}} = \frac{u \partial h / \partial x}{\partial h / \partial t} = \frac{u_o k}{\omega} = \frac{u_o}{C}, \quad (56)$$

876 the ratio of the fluid speed to the wave phase speed. This ratio arises very widely and is often called the
 877 Froude number,

$$878 \boxed{F = \frac{u_o}{C}} \quad (57)$$

879 Given the (tentative) scale estimate of the current amplitude, $u_o \approx C\eta_o/H$ (Sec. 3.1), the Froude
 880 number can be written in external parameters and easily evaluated (recall that for the base case, $\eta_o = 50$
 881 m and $H = 500$ m) as

$$882 F = \frac{\eta_o}{H} = 0.1.$$

883 The other nonlinear term in the thickness equation may be readily factored into nonlinear and linear
 884 terms, $h(\partial u / \partial x) = (\eta + H)(\partial u / \partial x)$. Under the assumption that the variable η will be no larger than
 885 the initial value η_o , then again

$$886 \frac{\text{nonlinear}}{\text{linear}} = \frac{\eta(\partial u / \partial x)}{H(\partial u / \partial x)} = \frac{\eta}{H} \approx \frac{\eta_o}{H}.$$

887 The important ratio, η_o/H , called simply the 'amplitude', happens to be equal to the Froude number in
 888 this case, but not generally. These simple estimates indicate that nonlinear terms are small but not

¹⁵This error can be made larger or smaller depending upon the smoothness of the initial condition. If allowed to grow unchecked, this grid scale noise can readily swamp the 'physical' content of a numerical solution, i.e., the part that is faithful to the model equations. A simple cure is to include the smallest possible horizontal diffusion of thickness and momentum that will serve to damp high frequency variability. That has been done in these numerical solutions, though mention of it was left out of the previous discussion. The issue then becomes whether this *ad hoc* diffusion impacts significantly the aspects of the solution that are of interest. In this experiment, a thickness diffusion $D = 5 \text{ m}^2 \text{ sec}^{-1}$ was sufficient to prevent runaway growth of the grid scale noise, though not enough to crush it completely. Over the short duration of this experiment, $T = 5$ days, this diffusion causes a small but acceptable spreading of the ridge judging from $\sqrt{DT^2} \approx 1.5 \text{ km} \ll L$.

negligible compared to comparable linear terms in the base case in which $\eta_o/H \approx 0.1$. It is then plausible, but not certain from this analysis, that there should occur modest but detectable finite amplitude effects in the corresponding numerical solution.

A complementary estimate of finite amplitude effects comes from considering that the gravity wave speed likely depends upon the actual fluid thickness, $h = H + \eta$ and not just the nominal thickness as in the linear wave speed, Eqn. (54). A wave pulse, which has one sign, might then propagate at a speed given by the average thickness taking account of the pulse amplitude,

$$C_{pulse} = \sqrt{g'(H + \eta_o/4)} \approx C(1 + \eta_o/8H), \quad (58)$$

in the specific case considered here. Taking this thickness-dependent view of wave speed one step further, the observed steepening appears to be consistent with the idea that the thickest part of a wave pulse should propagate faster than in the undisturbed fluid, which should in consequence produce a steepened wave pulse front.

3.6 Problems

(1) Some important things went by rather quickly in Sec. 3.2. You should verify that 1) any function whose argument is $(kx \pm \omega t)$ satisfies the elementary wave equation provided that $\omega/k = \sqrt{g'H}$, and 2) the initial data is satisfied by Eqn. (52) for any $\eta_o(x)$. However, if $\eta_o \ll H$ does not hold, then the assumption that the system is linear would not be appropriate.

(2) The analysis of Sec. 3.2 lead to the (plausible) hypothesis that the wave pulses found in the numerical solution have the properties and parameter dependence of elementary gravity waves (if not their expected appearance). How can you test this, given the opportunity to specify the parameters of new numerical experiments via `geoadj_1d.m` (Sec. 6.3)? For now, exclude finite amplitude effects by keeping the amplitude small, $\eta_o/H \leq 0.1$, say, and omit friction, which will be discussed below.

(3) Friction was omitted from the discussion of energy balance in Sec. 3.4, but it is included in the numerical model via a linear damping of the velocity, $-r\mathbf{V}$, sometimes called Rayleigh damping. In the solution shown here r was set to a small enough value that frictional effects were negligible. Some friction questions: 1) What value of r is required to damp an outgoing wave pulse to half initial amplitude as it arrives at $x = 500$ km? 2) How does the required r vary with the nominal layer thickness, H ? 3) Can you define a nondimensional number analogous to the Ekman number, $E = r/f$ (Part 1, Sec. 5) that serves to predict the amplitude of this damping effect?

(4) You can investigate finite amplitude effects systematically by experimenting with a much smaller and a much larger value for the initial thickness anomaly, say $\eta_o = 2$ and then $\eta_o = 200$ m (in the setup of the numerical model `geoadj_1d.m`). Some questions: 1) It is expected that finite amplitude effects should increase with η_o . But what if the nominal layer thickness, H , is increased apace with η_o so that the ratio, η_o/H remains constant? 2) Can you verify that wave front steepening (and rarefaction) is

923 large or small depending upon the Froude number, and conversely is independent of, e.g., the density
 924 difference, $\delta\rho$, when all else is held constant? 3) Does the scale for current speed, $C\eta_o/h$, account for
 925 the change in the actual (dimensional) current amplitude at small values of η_o/H ? How about at very
 926 large values of η_o/H ? 4) Test the estimated finite amplitude wave pulse speed Eqn. (58) using
 927 numerical solutions. 5) Instead of a ridge, suppose the initial interface displacement is a trough, $\eta_0 < 0$.
 928 Use the previous result 4) to explain the steepening and rarefaction seen in this case.

929 4 Geostrophic adjustment on an f -plane

930 The one new feature of the next experiment is that Earth's rotation is included in a simplified form, an
 931 f -plane, in which the Coriolis parameter is taken as a constant. The latitude is taken to be 30° N, and so

$$932 \quad = 2\Omega \sin(\text{latitude}) = \Omega = 7.292 \times 10^{-5} \text{ sec}^{-1}.$$

933 The inertial period is $2\pi/f \approx 1$ day (1 day less about 4 minutes). The one-dimensional domain and
 934 initial condition, including the initial state of rest, are unchanged from before.

935 We can compare the new experiment, Fig. (12), with the non-rotating experiment of the previous
 936 section, Fig. (10), and it is clear that the effects of rotation are very, very significant. We will discuss the
 937 details below, once we have a few more analysis tools in place. For now, note that there are still gravity
 938 waves that propagate away from the ridge, however their amplitude is much less than in the nonrotating
 939 case, and some wavelike motion persists for at least a week. The ridge subsides and spreads laterally in
 940 the first few days, but most of it remains in place, about 75% based upon a potential energy balance (Fig.
 941 15). There are counter-flowing currents whose direction is such that the Coriolis force tends to oppose
 942 the pressure gradient associated with the sloping layer thickness, i.e., $0 \approx f\nu - g'\partial\eta/\partial x$, and after only
 943 a few days, the remaining ridge is in approximate geostrophic balance. In this f -plane experiment, an
 944 exact geostrophic balance is possible in principle (though not, in general, in a numerical solution).

945 4.1 Dispersion relation for waves on an f -plane

946 The waves in this rotating experiment are clearly very different from the pure gravity waves of the
 947 nonrotating case. The dispersion relationship that links the wave frequency ω and the wave number k
 948 makes a concise and very useful characterization of their properties. To find the dispersion relation,
 949 postulate a plane wave with wave vector, $\mathbf{K} = k_x\mathbf{e}_x + k_y\mathbf{e}_y$, which has a magnitude
 950 $K = \sqrt{k_x^2 + k_y^2} = 2\pi/\lambda$ with λ the wave length. A propagating plane wave having frequency ω is then
 951 $u(x, y, t) = U \exp(i(k_x x + k_y y - \omega t))$ and similarly for v and η , where U, V, Γ are the constant but

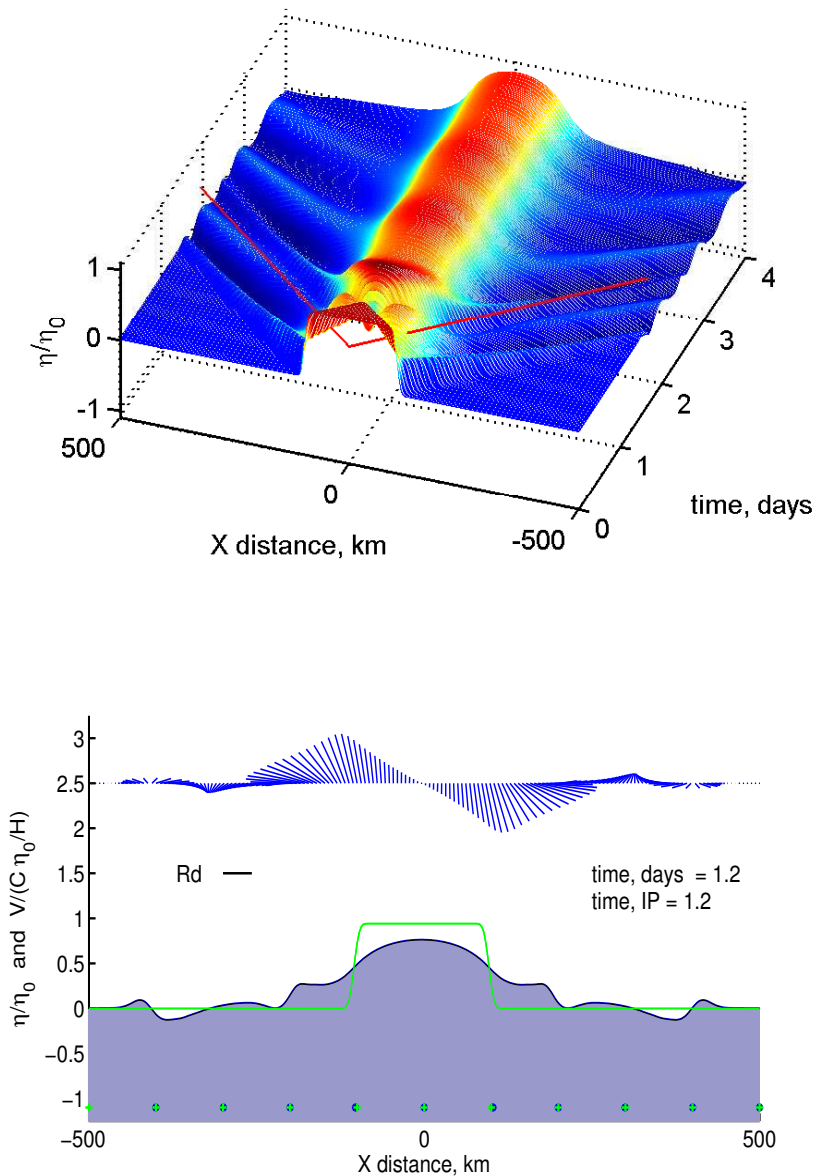


Figure 12: An experiment in geostrophic adjustment in one-dimension on an f -plane. **(upper)** The layer thickness anomaly, $\eta(x,t)/\eta_0$, of a rotating fluid layer following the release of a rectangular ridge having amplitude $\eta_0 = 50$ m. This solution was computed by the numerical model `geoadj_1d.m`. Time and horizontal distance are shown in days and kilometers to make a direct comparison with the nonrotating experiment shown in Fig. (10). The thin red lines have a slope given by the gravity wave speed, $C = \sqrt{g'H} = 275 \text{ km days}^{-1}$ in this case. **(lower)** A snapshot of the solution at $t = 1.2$ days. The green line shows the initial displacement η_0 . The current, which is shown by the array of vectors plotted above, is scaled with $C\eta_0/H = 0.30 \text{ m s}^{-1}$ for the parameters of this experiment. The blue dots and the green crosses at depth = -1.1 show the present and initial positions of floats. The floats do not move far in this experiment, and finite amplitude effects are small but detectable. Note the counter-flowing jets along the flanks of the partially subsided ridge. When the Coriolis force acting on these jets is sufficient to prevent the ridge from slumping further, the ridge is in a more or less steady, geostrophic balance. Animation: www.whoi.edu/jpweb/ga1-lat30.flv

952 unknown amplitudes of the velocity components and η . Substitution into the linear shallow water
 953 equations (30) and rewriting the resulting algebraic equations in a matrix format yields

$$954 \begin{bmatrix} -i\omega & -f & ig'k_x \\ f & -i\omega & ig'k_y \\ iHk_x & iHk_y & -i\omega \end{bmatrix} \begin{bmatrix} U \\ V \\ \Gamma \end{bmatrix} = 0. \quad (59)$$

955 This homogeneous system has nonzero solutions for $[U \ V \ \Gamma]$ only if it has a vanishing determinant,

$$956 \omega^3 - \omega(g'HK^2 + f^2) = 0, \quad (60)$$

957 which is to say, only if ω and K are related by a dispersion relation. The roots of (60) correspond to

$$958 \text{ steady, geostrophic motion : } \omega = 0, \text{ and} \quad (61)$$

$$959 \text{ gravity wave motion modified by rotation : } \omega = \pm \sqrt{g'HK^2 + f^2}. \quad (62)$$

961 Along with the dispersion relation, it is also helpful to find the polarization relation that relates the
 962 thickness and velocity components. Again we will presume a plane wave, but here there is no loss in
 963 assuming that propagation is in the x -direction only, i.e., $k_y = 0$. The thickness anomaly of a
 964 propagating plane wave can then be written $\eta(x, t) = \Gamma \cos(k_x x - \omega t)$. To find the corresponding $u(x, t)$
 965 we can eliminate v from Eqn. (30),

$$966 \frac{\partial^2 u}{\partial t^2} = -f^2 u - f \frac{\partial \eta}{\partial y} - \frac{\partial^2 \eta}{\partial x \partial t}. \quad (63)$$

967 Substitution of the presumed $\eta(x, t)$ into (63) then gives,

$$968 u(x, t) = \frac{k_x \omega}{f^2 - \omega^2} \Gamma \cos(k_x x - \omega t). \quad (64)$$

969 Similar treatment for the other velocity component yields

$$970 v(x, t) = \frac{k_x f}{f^2 - \omega^2} \Gamma \sin(k_x x - \omega t). \quad (65)$$

971 For the wave solution, $\omega > f$, the velocity vector rotates clockwise around an ellipse whose major axis
 972 is in the direction of the wavevector, here x , and whose major/minor axes is in the ratio

$$973 \frac{U}{V} = \frac{\omega}{f}.$$

974 Since $\omega \geq f$, the ellipse is more or less elongated or polarized in the wave vector direction depending
 975 upon frequency.

976 4.2 Intrinsic scales of the f -plane

977 The rotating, shallow water model has just three external parameters: the Coriolis parameter, f , that
 978 provides a natural time scale, the rotation time, $1/f$, noted in Part 1. The reduced gravity, $g' = g\delta\rho/\rho_o$,
 979 is an acceleration, and the layer thickness, H , a degenerate length scale since there is no variation over
 980 the layer. The initial condition adds two lengths, η_o and L . The Coriolis parameter f is an obvious
 981 (inverse) time scale for normalizing the frequency of the dispersion relation Eqn. (62), and thus a given
 982 frequency can be said to be high or low compared to f . By that rearrangement to nondimensional form
 983 the dispersion relation (62) then reads

$$984 \quad \frac{\omega}{f} = \pm \sqrt{\frac{g'H}{f^2}K^2 + 1}, \quad (66)$$

$$985 \quad = \pm \sqrt{R_d^2 K^2 + 1}, \quad (67)$$

986 in which the wavenumber K is automatically scaled by the very important length scale,

$$987 \quad \boxed{R_d = \frac{C}{f}}$$

988 called the radius of deformation. Just as f^{-1} is the intrinsic time scale of a rotating shallow water
 989 model, R_d is the intrinsic horizontal length scale of this model. It is often the case that the initial
 990 condition or external forcing bring an external length scale to the problem, in this case the ridge width L ,
 991 and the radius of deformation is the appropriate length scale for comparison. Thus a given ridge width
 992 is large or small as L/R_d is greater than or less than 1.¹⁶ After this very simple but significant
 993 rearrangement to nondimensional coordinates, the dispersion relation (Figs. 13 and 14) holds for all
 994 values of f , g' and H , i.e., for all shallow water, f -plane models.

995 The value of R_d depends upon the stratification through C and the latitude through f . Over the
 996 open, subtropical oceans, $C \approx 3 \text{ m sec}^{-1}$ and not highly variable; $C \approx 2 \text{ m sec}^{-1}$ at subpolar latitudes.
 997 The more significant geographic variation of R_d comes from the latitudinal variation of
 998 $f^{-1} \propto 1/\sin(\text{latitude})$. Notice that the equator is a special and an especially important case that will be
 999 considered in Part 3. In the ocean thermocline at 30°N , $R_d \approx 40 \text{ km}$. The R_d of the atmosphere at this
 1000 latitude is much larger, $R_d \approx 1000 \text{ km}$, because the atmosphere is both thicker than the ocean
 1001 thermocline, and more strongly stratified. This very large disparity in R_d is reflected directly in the
 1002 dominant horizontal scales of the variability seen in the atmosphere and ocean (cf. Figs. 1 of Part 1 and
 1003 Part 2), i.e., much larger horizontal scales are observed in the atmosphere.

¹⁶Four remarks. 1) A more compelling physical interpretation of R_d as a length scale will come just below. 2) The important ratio of frequencies, ω/f , is sometimes referred to as the temporal Rossby number, for which there seems to be no widely accepted symbol. 3) The ratio KR_d is the layered model equivalent of the square root of the Burger number, $B = N^2/f^2$,

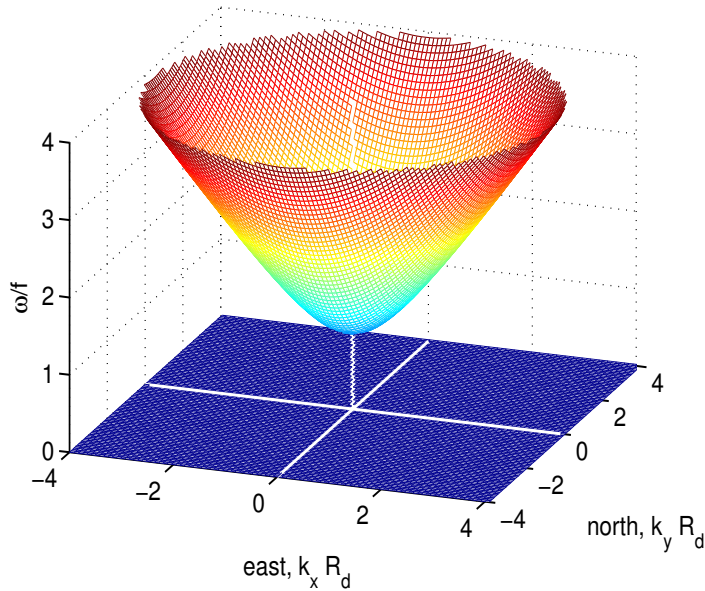


Figure 13: The dispersion relation for plane waves supported by the rotating, shallow water model. The frequency is normalized by the Coriolis parameter, f , and the wavenumber (an inverse length) by the inverse radius of deformation, R_d , discussed in the text. The colors are indicative of frequency only. A wavenumber vector \mathbf{K} having an origin at $(0, 0)$ and that terminates on either the bowl shaped surface or lies in the plane $\omega = 0$ is a solution, i.e., a possible free wave or geostrophic motion. This dispersion relation is symmetric about the ω axis (isotropic); the frequency of waves depends upon the magnitude of the wavenumber, \mathbf{K} , but not the direction of the wave vector.

1004 4.3 Gravity, inertial and geostrophic motions

1005 The non-zero ω/f root (the multi-colored parabola of Fig. 13 and the similar line of Fig. 14, upper)
 1006 corresponds to gravity waves that are modified by rotation. There are three important limits in the
 1007 dispersion relation that correspond with modes of the shallow water momentum equation.

1008 **High frequency, $\omega/f \gg 1$:** In the short wave, high frequency limit, say $\omega/f \geq 5$, the dispersion
 1009 relation asymptotes to pure gravity wave motion in which the phase and group speed are $C = \sqrt{g'H}$, as
 1010 in the non-rotating, shallow water model (Sec. 3.1).¹⁷ Pure gravity waves have the fastest group speed,
 1011 $C_g \approx C$, and would be expected to arrive first in the far field, just as observed in the numerical solution.
 1012 For these waves, the velocity is fairly strongly polarized in the direction of the wave propagation, as
 1013 $U/V = \omega/f$, which may be called longitudinal.

1014 **Inertia-gravity waves: $1 < \omega/f < 5$** Intermediate scale waves fall somewhere between the limiting
 1015 cases of pure gravity wave and pure inertial oscillation ($\omega/f = 1$, coming next), and are appropriately
 1016 called inertia-gravity waves (or, rarely, gravity-inertia waves). Their phase speed depends upon K .

where $N^2 = (g/\rho)(\partial\rho/\partial z)$ is the static stability, times the aspect ratio H/λ . 4) There is no guarantee that the value 1 will always mark the boundary between large and small values of a given nondimensional number as factors of π or even $2\pi^2$ are sometimes relevant.

¹⁷If the wavelength is less than the layer thickness, H , then the wave motion will become a short gravity wave that is surface-trapped. These are the high frequency, wind-generated waves that make up most of the sea state and they are outside the domain of the shallow water model. Their frequency can be high enough that the pressure is nonhydrostatic.

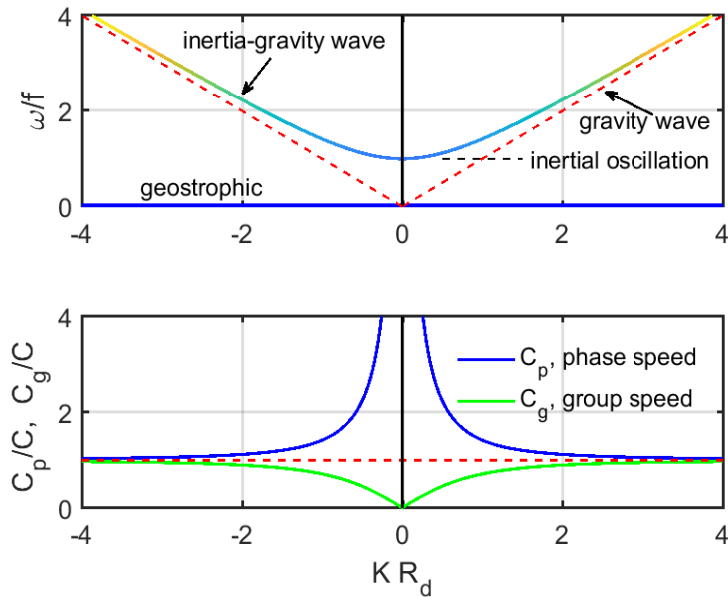


Figure 14: **(upper)** The dispersion relation for plane waves supported by the rotating, shallow water model. This is a slice through the isotropic surfaces of the previous figure. The blue line at zero frequency is the steady, geostrophic solution and the multi-colored parabola is the dispersion relation for inertia-gravity waves. The straight red dashed lines are for pure gravity waves ($f = 0$); in these nondimensional coordinates their slope is ± 1 for right- and left-going waves. **(lower)** The phase and group speeds of the inertia-gravity waves (blue and green lines) normalized by the gravity wave speed, C . Inertia-gravity waves are dispersive in that their phase speed varies with K . For short waves, $KR_d \gg 1$, the group speed asymptotes to that of pure gravity waves (the dashed red line) and in that limit $C_g = C_p = C$. The group speed goes to zero for very long waves, $KR_d \ll 1$, that have frequencies near f , i.e., near-inertial oscillations. The phase speed becomes infinite as $KR_d \rightarrow 0$.

1017 Hence the inertia-gravity waves of an f -plane are dispersive, so that the shape of $\eta_0(x)$ is not, in
 1018 general, preserved as these waves propagate away from a source (cf. the nonrotating, pure gravity wave
 1019 experiment of Sec. 3.1). Instead, the initial form $\eta_0(x)$ will become more or less spread out, or
 1020 'dispersed', over time as waves of different wavelengths propagate at different C_g .¹⁸

1021 **Lowest possible wave frequency, $\omega/f \downarrow 1$:** In the long wave limit, i.e., as KR_d becomes very small,
 1022 inertia-gravity waves asymptote to inertial oscillations and the frequency approaches f . In this limit the
 1023 phase speed is very large, infinite at $\omega/f = 1$. The entire field of motion consists of clockwise-rotating
 1024 velocity having uniform phase, and thus no divergence and no associated η or pressure anomaly. It is
 1025 appropriate to call this an inertial oscillation, to distinguish from vortical inertial motion that we will
 1026 see in Sec. 5. Exact inertial oscillation, like exact geostrophic motion, amounts to a kind of frozen state
 1027 that is unable to evolve. Consistent with this, the group speed in the limit $\omega/f \rightarrow 0$ is zero. Exact

¹⁸The linear initial value problem can also be solved usefully via Fourier transform. An example is carried out by the script transform.m (Sec. 6.3), which allows the choice of a dispersion relation. Somehow one must specify what fraction of the initial thickness anomaly will be dispersed into waves: in the non-rotating gravity wave case, all of the initial thickness anomaly η_o goes into propagating waves, but in the rotating case, a more or less significant fraction of η_o remains in the geostrophically balanced end-state as we will discuss shortly.

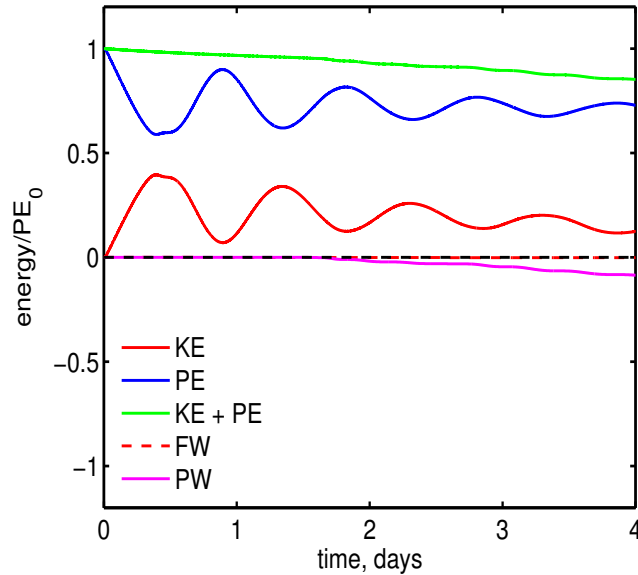


Figure 15: Energy balance of the f -plane geostrophic adjustment problem evaluated over $-500 \leq x \leq 500$ km. The energy and work terms are nondimensionalized with the initial potential energy, PE_0 , and time is in days. At 30° N, 1 day \approx 1 inertial period. These data may be compared directly with that of the non-rotating experiment (Fig. 11) and are remarkably different. In this rotating experiment, very little energy was radiated out the sides of the domain, $PW \ll KE + PE$, and was instead retained within the geostrophically balanced ridge as potential energy, mainly, plus significant kinetic energy. Notice that the decrease of total energy is slightly greater than the wave radiation through the sides, evidence of a small but likely growing numerical error.

1028 inertial motion requires an infinite horizontal scale, and hence can not be realized in a finite ocean basin,
 1029 or for any number of other reasons, e.g., the latitudinal variation of f and the existence of other ocean
 1030 currents. While exact inertial oscillations are not expected in the ocean, rotary currents that turn in the
 1031 direction of an inertial motion and that have frequencies within 5-10 percent of f — near-inertial
 1032 oscillations — are very common, for example whenever there is a rapidly changing wind stress on the
 1033 ocean surface (an example was noted in Section 5 of Part 1).

1034 Notice that there is a low frequency range, $0 < \omega < f$, within which there are no free motions
 1035 possible in this f -plane system.

1036 **Steady, geostrophic motion, $\omega = 0$:** The root $\omega/f = 0$ corresponds to exactly steady, geostrophic
 1037 motion (the blue plane of Fig. 14, upper). In this f -plane model, the corresponding wavenumber can
 1038 have any orientation and any magnitude (this will not be true when the latitudinal variation of f is
 1039 acknowledged in Part 3). At first this may seem a trivial solution, but it is instead the f -plane
 1040 approximation of the slowly-varying and nearly geostrophic motion that makes up most of the
 1041 atmosphere and ocean circulation. The polarization relation shows that the velocity associated with a
 1042 plane wave thickness anomaly (not propagating) is solely in the y direction, parallel to constant
 1043 thickness, and perpendicular (transverse) to the wave vector.

1044 4.4 The steady state inferred from potential vorticity conservation

1045 The dispersion relation is an invaluable guide to the properties of the waves that arise in a geostrophic
 1046 adjustment experiment, but it can't tell us everything we might want to know. For example, the
 1047 dispersion relation alone gives no hint to the amplitude of any process, i.e., it does not tell how much of
 1048 the initial ridge will disperse into waves vs. survive into a geostrophic steady state. Notice too that a
 1049 given wavenumber in Fig. (13) can be either a time-dependent wave, or, a steady geostrophic motion.
 1050 What distinguishes these two very different kinds of motion? These important questions lead to an
 1051 analysis of potential vorticity conservation, described next.

1052 A key result of this experiment is that most of the ridge survived the adjustment process, e.g.,
 1053 about 75% of the initial potential energy (Fig. 15). The conservation of potential vorticity provides real
 1054 insight into why this was the case in this experiment, and why it will not be in others. In words, the
 1055 q -conservation law Eqn. (29) states that q of a parcel (column) is unchanged by the process of
 1056 geostrophic adjustment, or,

$$1057 \quad q(\alpha) = q_o(\alpha), \quad (68)$$

1058 where α is a parcel tag. Assuming that q_o is known, then the task is to follow the parcels (all of the
 1059 parcels) during the adjustment process. However, if the amplitude is small in the sense that parcel
 1060 displacements are small compared to the scales over which the currents vary significantly, then a very
 1061 helpful approximation of (68) is that

$$1062 \quad q(x) = q_0(x), \quad (69)$$

1063 with x the usual (Eulerian) spatial coordinate. In other words, if the horizontal displacements during the
 1064 adjustment process are small, then q will be conserved in place, approximately, and q conservation is
 1065 linear. This may be checked by comparing the horizontal displacement of floats against the width of the
 1066 adjusted portion of the ridge. In the base case (Fig. 12) there is a detectable, outward displacement of
 1067 floats during the adjustment process, but the float displacement is small compared to the width of the
 1068 adjusted portion of ridge, the radius of deformation, discussed below. As well, the geostrophic currents
 1069 that form along the edge of the adjusted ridge are in a direction that is perpendicular to the thickness
 1070 and velocity gradients and so cause no horizontal advection. The result is that q is indeed conserved in
 1071 place, approximately, (Fig. 16, upper) as presumed in Eqn. (69). Note that the changes of v and η that
 1072 occur during adjustment are significant so that linear q conservation is by no means trivial (Fig. 16).

1073 The potential vorticity in this one-dimensional (x -dependent only) case is just

$$1074 \quad q = \frac{f + \partial v / \partial x}{H + \eta}.$$

1075 The initial state included the ridge within which the layer thickness was $H + \eta_0$, and elsewhere the
 1076 thickness was H . The ridge was presumed to be at rest, and so the initial relative vorticity vanishes. The

1077 q distribution in the initial and in the final state is then, within the initial ridge,

$$1078 \quad \frac{f + \partial v / \partial x}{H + \eta} = \frac{f}{H + \eta_0} \quad \text{if } |x| \leq L, \quad (70)$$

1079 and outside of the ridge

$$1080 \quad \frac{f + \partial v / \partial x}{H + \eta} = \frac{f}{H} \quad \text{if } |x| > L. \quad (71)$$

1081 Note that both $v(x)$ and $\eta(x)$ are unknowns, but in addition, we have come to expect that the steady
1082 state should be in geostrophic balance, and hence we have also the geostrophic relationship between v
1083 and η , viz.

$$1084 \quad 0 = f v_{geo} - g' \frac{\partial \eta_{geo}}{\partial x}.$$

1085 When this v_{geo} is substituted into the q conservation law, say for the region $x \geq L$, Eqn. (71), there
1086 follows a second order, ordinary differential equation in $\eta_{geo}(x)$:

$$1087 \quad \frac{g'H}{f^2} \frac{d^2 \eta_{geo}}{dx^2} - \eta_{geo} = 0.$$

1088 The boundary conditions on η may be applied over four segments, $x \leq -L$, $-L < x \leq 0$, $0 < x \leq L$
1089 and $x \geq L$. For example for the right-most segment, $x \geq L$, the boundary conditions are

$$1090 \quad \eta_{geo}(L) = \eta_0/2 \quad \text{and} \quad \eta_{geo}(\infty) = 0.$$

1091 The solution for this segment only is then

$$1092 \quad \eta_{geo}(x) = \frac{\eta_0}{2} \exp\left(-\frac{x-L}{R_d}\right). \quad (72)$$

1093 By matching the solutions of the four segments, $\eta_{geo}(x)$ may be constructed across the entire ridge with
1094 a result that compares fairly well with the the numerical solution (Fig. 16, middle). Two notable
1095 features of this solution:

1096 **1) The horizontal length scale is R_d :** Compared with the initial ridge, the adjusted ridge is 'deformed'
1097 over the horizontal e-folding scale R_d . The width of the adjusted portion of the ridge is then about $3R_d$.
1098 This result suggests a clear physical interpretation of R_d . Recall from Part 1, Sec. 5.3 that $1/f$ is the
1099 time it takes for rotation to turn a parcel (started from rest) by one radian with respect to an
1100 impulsively-applied force. R_d is then the distance that a gravity wave will propagate in the time $1/f$,
1101 and hence R_d is proportional to the distance that the ridge will spread outward (as a gravity wave)
1102 before being arrested by the Coriolis force. Implicit in this is a definite meaning to the phrase 'large
1103 scale' as applied to a mass anomaly of half-width or radius L : the appropriate standard against which to
1104 compare (or measure) a horizontal length is R_d . The radius of deformation varies quite a lot with
1105 latitude, as noted earlier, and is very large (though not infinite) as f vanishes. The nonrotating

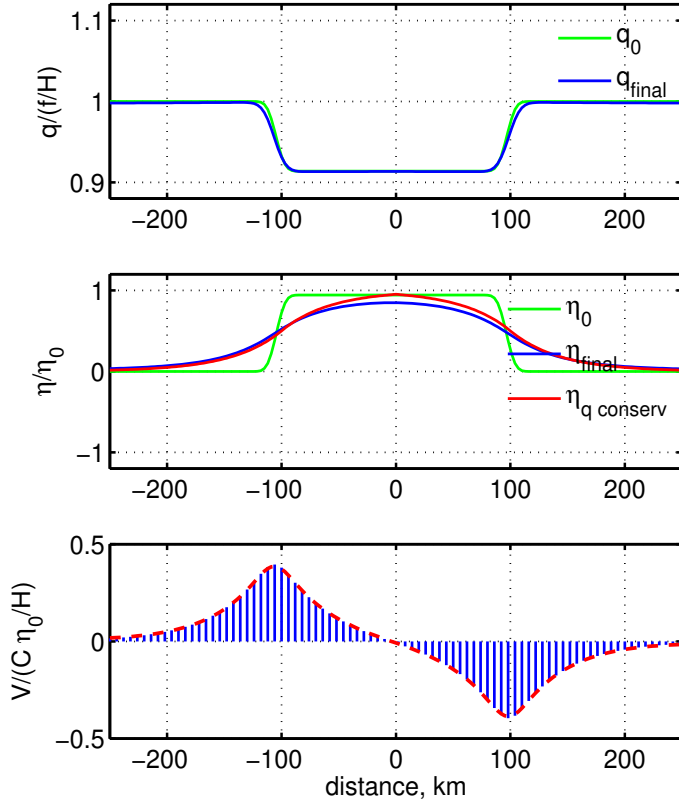


Figure 16: Elements of the potential vorticity balance for the f -plane geostrophic adjustment experiment. **(upper)** Initial (green) and final (blue) $q(x)$ (the latter is at $time = 6$ days). Note that q of the numerical solution is almost unchanged by the process of geostrophic adjustment, as should have been the case, despite that there are large changes in the thickness and the current. **(middle)** The initial and final thickness anomaly (green and blue lines). The red line, η_{geo} , is the steady state thickness anomaly computed from Eqn. (72) under the assumption of geostrophy and q conservation. **(lower)** Time-mean current (blue vectors). The velocity maxima, or jets, at $x = \pm 100$ km $= \pm L$, coincide with the adjusted part of the initial ridge. These jets are in a near geostrophic balance as evidenced by a very close match with the geostrophic velocity, $(g'/f)\partial\eta_{final}/\partial x$ (dashed red line).

1106 (gravitational) adjustment experiment of Sec. 3 can now be seen as the limit $R_d/L \rightarrow \infty$ in which
 1107 rotational effects are expected to be negligible — literally zero in that case — compared to the
 1108 spreading of an unbalanced thickness anomaly by gravity wave processes.

1109 **2) q -conservation and the geostrophic jets:** The result Eqn. (72) gives an essentially complete
 1110 account of the geostrophic jets. The jets have a relative vorticity $\partial v/\partial x$ (Fig. 16, lower) that follows
 1111 from the effect of column thickness change and q conservation. For example, over the right-most
 1112 segment, $x > L$, the layer thickness increased (the water column was stretched) from H to $H + \eta(x, t)$
 1113 during the adjustment process (Fig. 16, middle). The initial potential vorticity was just f/H since there
 1114 was no initial velocity and no relative vorticity. To maintain constant q during the adjustment process,
 1115 the relative vorticity $\xi = \partial v_{geo}/\partial x = f\eta/H > 0$ of the jet must thus be positive, or cyclonic, in this
 1116 region. Stretching of the water column appears to produce positive relative vorticity by concentrating
 1117 the planetary vorticity (Fig. 5, upper). To an Earth-bound, rotating observer, who sees stars turning
 1118 overhead but not the rotation due to planetary velocity, it looks as if this relative vorticity has come out
 1119 of nowhere. To an inertial observer for whom the same stars stand still, this looks like familiar angular
 1120 momentum conservation, albeit of a deformable object.

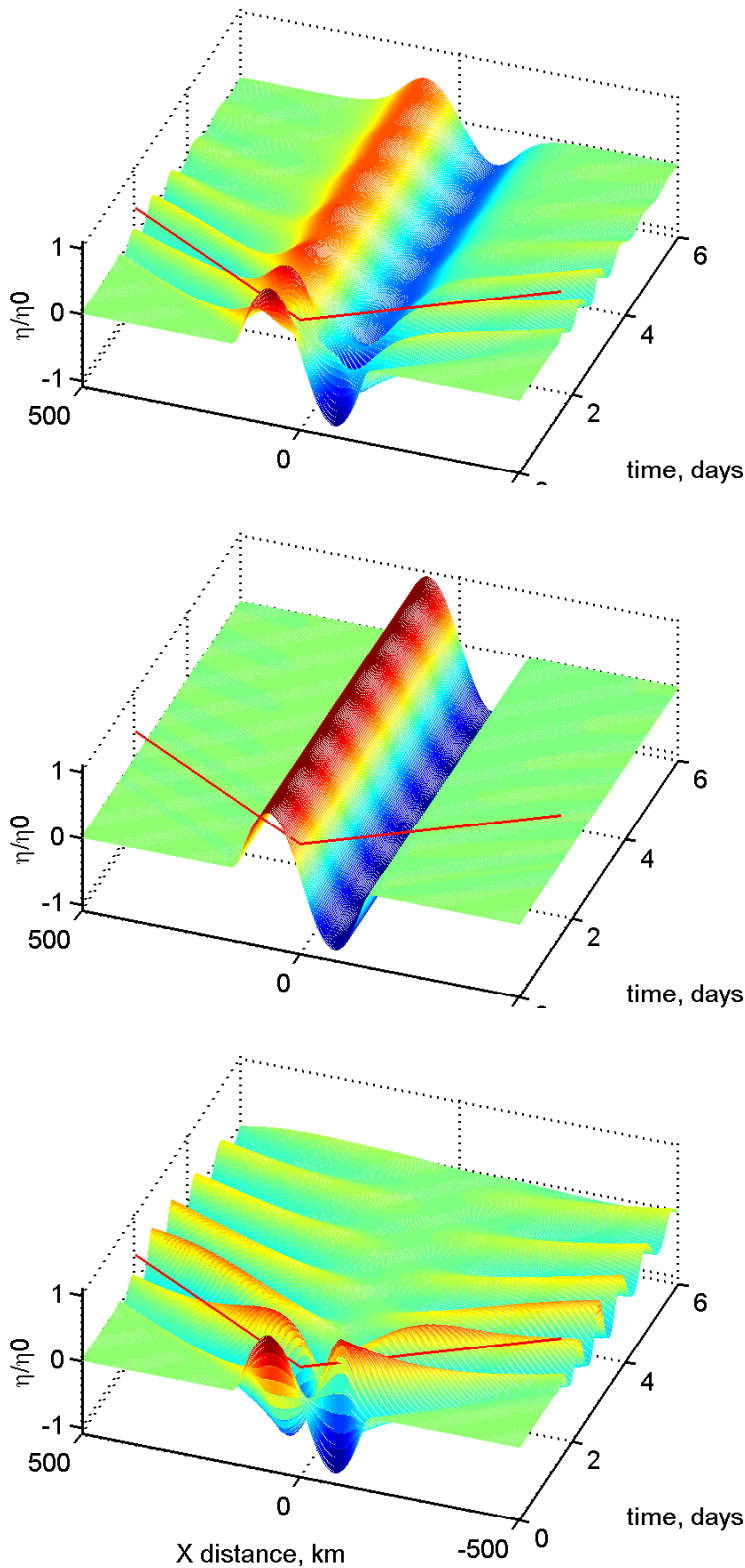


Figure 17: Three experiments in geostrophic adjustment in which the initial thickness anomaly was a single wave $\eta_0 \sin(\pi x/L)$. The initial velocity was either **(top)** vanishing, as in the previous experiments, **(middle)** geostrophically balanced with the initial thickness anomaly, in which event nothing happens when the ridge is released, or **(bottom)** the velocity that gave vanishing q anomaly with respect to the outlying fluid. In this last case all of the initial ridge is dispersed by inertia-gravity waves; there is no geostrophic steady state. These experiments were carried out with `geoadj_1d_uic.m`, linked in Sec. 6.3. An animation of this last case is www.whoi.edu/jpweb/zeroq1d.mp4

1121 4.5 If there is no potential vorticity anomaly

1122 Note that if the initial q was spatially uniform (no q anomaly) the geostrophic, q -conserving solution
 1123 (72) would be $\eta(x) = 0$, i.e., vanishing geostrophic steady state. In the experiment just described the
 1124 initial ridge was a q anomaly because the initial velocity was assumed to vanish and hence the q of the
 1125 initial ridge was $f/(\eta_o + H)$ compared with f/H outside the ridge. A vanishing initial velocity is the
 1126 simplest initial state to define and a reasonable place to start experimenting, but it is not necessarily the
 1127 most realistic or common initial condition. An experiment that allows a more general initial condition
 1128 that includes velocity will make clear that insofar as the possible steady (adjusted) state is concerned,
 1129 the initial ridge is defined by q its anomaly, generally, and not by η alone, as it may have seemed from
 1130 this first rotating experiment.

1131 For this more general case it is preferable to assume an initial $\eta_o(x)$ that has zero mean (though
 1132 still called a ridge), e.g.,

$$1133 \quad \eta(x, t = 0) = \eta_o \sin(\pi x/L) \text{ if } |x| < L, \text{ and } \eta(x, t = 0) = 0 \text{ otherwise.}$$

1134 Now consider one of three initial velocity fields that vanish outside of the thickness anomaly:

1135 vanishing velocity, $V(x, t = 0) = 0$, just as before,

1136 geostrophic velocity, $V(x, t = 0) = (g'/f)\partial\eta(x, t = 0)/\partial x$, or,

$$1137 \quad \text{vanishing } q \text{ anomaly } V(x, t = 0) = \int_{-L}^x f\eta(x, t = 0)/H dx.$$

1140 The first of these experiments (Fig. 17, upper) is very much like our previous experiment in that about
 1141 two thirds of the initial ridge survives into a steady, geostrophic state. The second experiment is a
 1142 non-event (Fig. 17, middle); nothing happens when a geostrophically-balanced ridge is released onto an
 1143 f -plane (this would not be true if the latitudinal variation of f was retained, Part 3).

1144 The third experiment is the important and perhaps surprising one: a ridge having zero q anomaly is
 1145 completely dispersed by inertia-gravity waves, with nothing surviving into a steady state (Fig. 17,
 1146 lower). This holds regardless of the width of the ridge. Evidently the width of a ridge is best defined
 1147 from its q anomaly, and not by width alone, insofar as the existence of a steady state is concerned. This
 1148 last experiment, vanishing initial q anomaly, may seem a special, contrived case, but in fact it is very
 1149 common: tidal waves in the open ocean have large spatial scales, wavelengths of hundreds to thousands
 1150 of kilometers, and yet tidal waves propagate as almost free waves that show no sign of adjusting to the
 1151 kind of geostrophic balance that characterizes mesoscale eddies and gyres. The reason is that tidal
 1152 waves are generated by a small gravitational/centrifugal imbalance, the tidal force, that does not exert a
 1153 torque and so does not by itself generate a potential vorticity anomaly. Thus the difference between
 1154 two identical wavenumbers (Fig. 13), one being a steady geostrophic motion and the other being a
 1155 wave, is evidently the association (or not) of a potential vorticity anomaly.

1156 4.6 Problems

1157 (1) Geostrophic balance is the final, steady state of the experiment in Fig. (12). How long would you
 1158 say it takes for geostrophy to hold in this experiment? Recall from Part 1 that the time scale required for
 1159 rotation to deflect a moving parcel significantly was $1/f \approx 1/4$ days at mid-latitudes. On the other
 1160 hand, energetic near-inertial oscillations evidently persist for roughly five days. Are you thinking about
 1161 an instantaneous geostrophic balance, or a time-mean geostrophic balance?

1162 (2) Go back to the linear shallow water system Eqns. (30) and identify which of the terms are relevant
 1163 in each of the three limits of the dispersion relation discussed in Sec. 4.3.

1164 (3) Using the Matlab scripts `geoadj_1d.m` and `geoadj_1d_uic.m` to generate new solutions, 1) find
 1165 experimentally how the width of a geostrophic jet varies with latitude and with H and g' . What do you
 1166 expect if the latitude is from the southern hemisphere? Before trying these experiments in the numerical
 1167 model, do a thought experiment and test your developing intuition against the numerical solution.

1168 (4) Show that a plausible velocity scale for a geostrophic jet is $C\eta_o/H$. How/why does the jet speed
 1169 vary with H ? Show that a reasonable *a priori* estimate of parcel displacement is $C\eta_o/Hf$ and that the
 1170 condition for linearity with respect to horizontal advection is then the familiar one, $\eta_o/H \ll 1$. Suppose
 1171 that the initial thickness anomaly is made very large, say $\eta_o = 200$ m. How does this alter the potential
 1172 vorticity balance during the adjustment process?

1173 (5) The power of the potential vorticity analysis becomes evident when one considers different kinds of
 1174 initial conditions, say $\eta_o = 0$, but with an unbalanced current, $u = u_o$ if $|x| \leq L$, and otherwise $u = 0$
 1175 (recall that u is the velocity component in the x -direction). Then assume the same profile but with the
 1176 initial velocity directed in the y direction. Which of these initial states has vorticity, and thus a potential
 1177 vorticity anomaly that should remain in the adjusted state? Solutions for these initial velocity
 1178 distributions can be generated by `geoadj_1d_uic.m`.

1179 (6) The solution shown here in Sec. 4 was made with a vanishingly small value of the linear damping
 1180 coefficient. What happens to the wave response and to the geostrophic currents when damping is made
 1181 significant? Connect the results you obtain here with the Ekman number developed in Part 1, Sec. 5.

1182 5 In two dimensions

1183 In this section we will consider briefly a two dimensional f -plane geostrophic adjustment experiment
 1184 that introduces one new effect, flow curvature, and an important new nondimensional number, the
 1185 Rossby number, that measures its magnitude. Aside from being two-dimensional, the configuration is
 1186 unchanged from the basic case of Sec. 4: the initial thickness anomaly is taken to be a right cylinder
 1187 having a radius $L = 100$ km that is typical of mesoscale eddies, and an amplitude 100 m. The

1188 stratification and central latitude are as before, $H = 500$ m, $g' = 2 \times 10^{-2}$ m sec⁻¹ and hence
 1189 $C = \sqrt{g'H} \approx 3.2$ m sec⁻¹ (about 300 km day⁻¹), and $f = 7.29 \times 10^{-5}$ sec⁻¹.¹⁹

1190 5.1 Adjustment

1191 The slumping of the thickness anomaly produces inertia-gravity waves that propagate isotropically
 1192 away from the center (cover graphic). The dispersion properties of these waves are familiar from the
 1193 one-dimensional f -plane case. The wave front expands at a rate very close to the gravity wave speed,
 1194 about 300 km day⁻¹ (Fig. 1). The amplitude at the wave front is a small fraction of η_0 , and decreases
 1195 with time due to geometric spreading $\propto 1/r$ (not present in one dimension). The frequency at the wave
 1196 front is roughly $2f$, and the current is at first polarized in the radial direction. With increasing time, the
 1197 frequency decreases toward f , and the current vector rotates as a near-inertial motion. Near the initial
 1198 eddy, weak near-inertial motion persists for several weeks.

1199 Most of this eddy remained in place after the geostrophic adjustment process was essentially
 1200 complete, several weeks after start. The resulting current was then nearly steady and anti-cyclonic
 1201 (clockwise) around the eddy center, a high (Fig. 18). The initial condition was azimuthally symmetric,
 1202 and nothing about the f -plane dynamics would change that (not the case when the β -effect is
 1203 acknowledged, Part 3). Potential vorticity and energy balances are as expected from the
 1204 one-dimensional cases of Sec. 4; e.g., potential vorticity stays with the fluid as prescribed in the initial
 1205 condition.

1206 5.2 Curvature and Rossby number

1207 Once the motion reaches an azimuthally symmetric steady state we can diagnose some of its properties
 1208 using the single parcel model of Part 1 (though, of course, we could not use the single parcel model to
 1209 calculate the adjustment process in the first place). The radial component equation of motion for a
 1210 rotating, polar system is (Part 1, Sec. 3.1, Eqn. 40)

$$1211 \quad \frac{d^2 r}{dt^2} - r\omega^2 = r\Omega^2 + 2\Omega\omega r + F_r/M,$$

where we have dropped the primes used in Part 1 to indicate a rotating reference frame. The upper case Ω is the rotation rate of the reference frame, and the lower case ω is that of the parcel. Given that the flow is in steady state, the radial acceleration vanishes. The centrifugal force due to the reference frame

¹⁹The numerical model used to solve these two dimensional problems is written in Fortran, `geoadj_2d.for`, linked in Sec. 6.3.

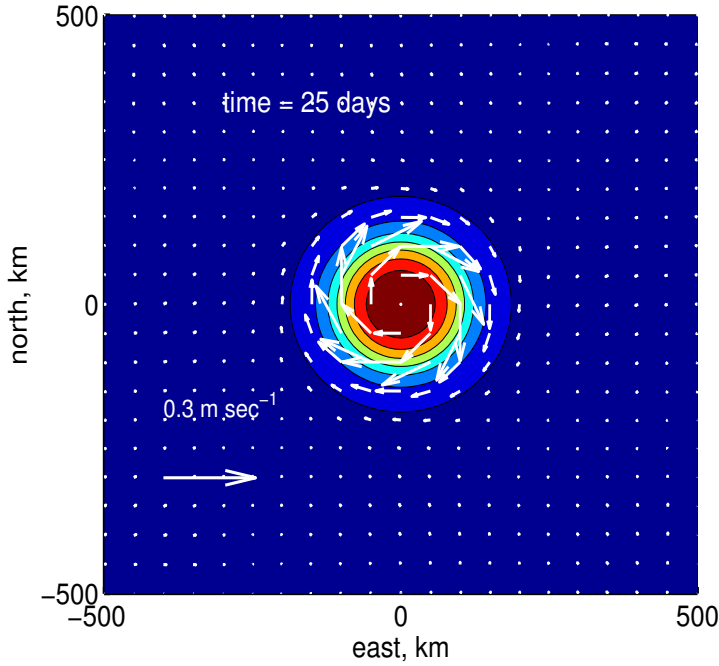


Figure 18: Velocity and interface displacement (color contours) from a two-dimensional f -plane experiment. This is a snapshot at 25 days. This eddy is a high in thickness (about 70 m at the center) and pressure and so the balanced flow is anti-cyclonic (clockwise). The big vector at lower left has a magnitude $0.5C\eta_0/H = 0.3 \text{ m sec}^{-1}$ and serves as a speed scale.

rotation (first term on the right) also vanishes (as described in Part 1, Sec. 3). The azimuthal current is $U_\lambda = \omega r$, $f = 2\Omega$, and the external force F is the radial pressure gradient, $\propto \partial\eta/\partial r$. With these identifications, the equation of motion is

$$-\frac{U_\lambda^2}{r} = fU_\lambda - g' \frac{\partial\eta}{\partial r},$$

in which the centripetal acceleration equals the sum of the Coriolis force and the pressure gradient. It is easier to envision the steady force balance that would follow from adopting a co-rotating frame in which the parcel is not accelerating. In that case, the equation of motion is

$$0 = \frac{U_\lambda^2}{r} + fU_\lambda - g' \frac{\partial\eta}{\partial r}. \quad (73)$$

1212 The Coriolis force will be positive (outward) if the current is cyclonic, or negative (inward) if the flow is
 1213 anticyclonic. The pressure gradient force, $\propto -\partial\eta/\partial r$, may also have either sign, positive if a high, and
 1214 negative if a low. If the balance was just between these two terms, then the velocity would be the
 1215 geostrophic velocity,

$$1216 \quad U_\lambda = U_{geo} = \frac{g'}{f} \frac{\partial\eta}{\partial r}.$$

1217 The interesting term is the centrifugal force which is always positive (always outwards), with
 1218 important consequences. The magnitude of the centrifugal force may be assessed by comparison to the

1219 Coriolis force,

$$1220 \frac{\text{centrifugal}}{\text{Coriolis}} = \frac{U_\lambda^2/r}{fU_\lambda} = \frac{U_\lambda}{fr},$$

1221 often written

$$1222 \boxed{R_o = \frac{U_\lambda}{fr}} \quad (74)$$

1223 an important nondimensional number called the Rossby number.²⁰ To estimate R_o for this eddy we
 1224 could use the initial radius, $r = 100$ km, where the current is strongest (Fig. 18), and an estimate of the
 1225 current, $U_\lambda \approx -0.2$ m s⁻¹, negative since clockwise or anticyclonic: $R_o \approx -0.03$. The centrifugal force
 1226 is thus very small compared to the Coriolis force. In some applications the sign of R_o has no
 1227 significance, but here it does if we use R_o to rewrite Eqn. (73),

$$1228 0 = fU_\lambda(1 + R_o) - g \frac{\partial \eta}{\partial r},$$

1229 or,

$$1230 U_\lambda = \frac{1}{1 + R_o} U_{geo}.$$

1231 In the case of a high pressure, anti-cyclone, Fig. (18), the centrifugal force adds constructively to the
 1232 pressure gradient force, and in steady state, this combined centrifugal plus pressure gradient force must
 1233 be balanced by a centripetal Coriolis force. The magnitude of the azimuthal velocity in a steady, high
 1234 pressure anticyclone exceeds the geostrophic speed by a factor $1/(1 + R_o) \approx 1.03$. Such a small effect
 1235 of curvature is not apparent in Fig. (18) but evident on closer inspection, Fig. (19). A steady flow in
 1236 which geostrophy is modified by curvature in this way is said to be in gradient balance or sometimes
 1237 just 'balanced', with geostrophy modified by curvature being understood.

1238 In the case of our nominal oceanic mesoscale eddy the effects of curvature are, admittedly, not
 1239 compelling. What is considerably more interesting is the insight that the gradient balance (73) can
 1240 provide regarding eddies generally. To that end we can treat Eqn. (73) as a quadratic equation for the
 1241 unknown U_λ and with parameters f , r and $-g' \frac{\partial \eta}{\partial r}$;

$$1242 U_\lambda = \frac{-f \pm \sqrt{f^2 + \frac{4g'}{r} \frac{\partial \eta}{\partial r}}}{2/r}. \quad (75)$$

1243 This is a little difficult to interpret and can benefit from streamlining by dimensional analysis. There are
 1244 four variables or parameters having two fundamental dimensions, length and time. Hence it should be

²⁰This is a specific form of Rossby number. A more general form could be written $R_o = U/fL$, where U is a characteristic velocity (whose sign is usually not relevant), and L is the spatial scale over which the velocity varies significantly. For example, the ratio of momentum advection to the Coriolis force in the shallow water model is $U(\partial U/\partial x)/fU \approx (U^2/L)/fU = U/fL = R_o$, where equality here means same order of magnitude. Small R_o thus implies a small magnitude of momentum advection compared to the Coriolis force. An assertion of small R_o is often made at the start of a linear approximation.

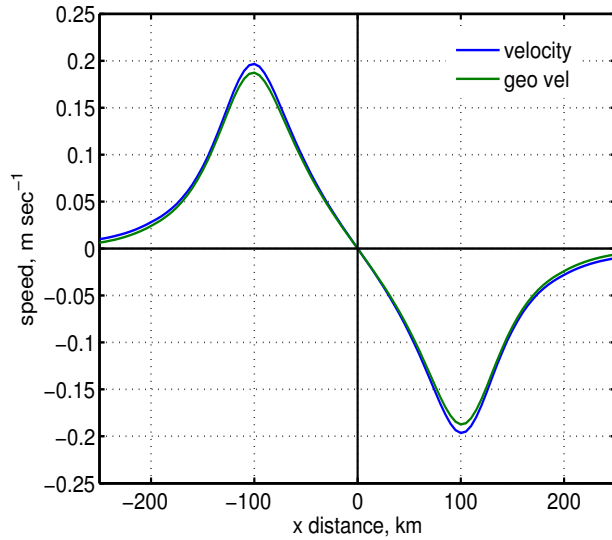


Figure 19: A slice across the adjusted eddy of Fig. (18). The geostrophic north-south velocity computed from the thickness field is the green line and the actual velocity is the blue line. The actual velocity of this high, anticyclone is only very slightly larger than the geostrophic velocity, just as expected from the small Rossby number, $R_o \approx -0.03$.

1245 possible to rewrite (75) in terms of one nondimensional dependent variable, and one nondimensional
 1246 parameter. One possibility is

$$1247 \quad R_o = \frac{U_\lambda}{fr} = -\frac{1}{2} \pm \sqrt{\frac{1}{4} - \Pi}, \quad (76)$$

1248 plotted as the blue and red lines in Fig. (20). The dependent variable is the Rossby number (74), and the
 1249 independent variable is, from the second term in the radical of Eqn. (75),

$$1250 \quad \Pi = -\frac{g' \partial \eta}{rf^2 \partial r},$$

1251 the nondimensional pressure gradient. The normalizing factor is rf^2 , the centripetal acceleration of an
 1252 inertial motion. The signs of R_o and Π are significant: $R_o > 0$ indicates a cyclonic (anticlockwise) flow,
 1253 while $\Pi > 0$ indicates high pressure, which, if geostrophic, would be anticyclonic.

1254 There are several noteworthy features of (76):

1255 1) The upper left quadrant ($\Pi > 0$ and $R_o \geq 0$) of Fig. (20) is empty. There is no steady, gradient
 1256 balance for a high pressure cyclone, since all three of the forces in such an eddy would be outward.

1257 2) The large negative Π solutions, say $\Pi < 1$, are low pressure eddies for which the flow can be of
 1258 either sign. For these intense eddies, the Coriolis force is of little importance, and the balance is mainly
 1259 between the pressure gradient (inward) and the centrifugal force (outward), a so-called cyclostrophic
 1260 balance. Tornadoes are the star examples from nature, but cyclostrophic eddies or vortices abound in
 1261 everyday flows for which the spatial and time scales are small enough that the Coriolis force is

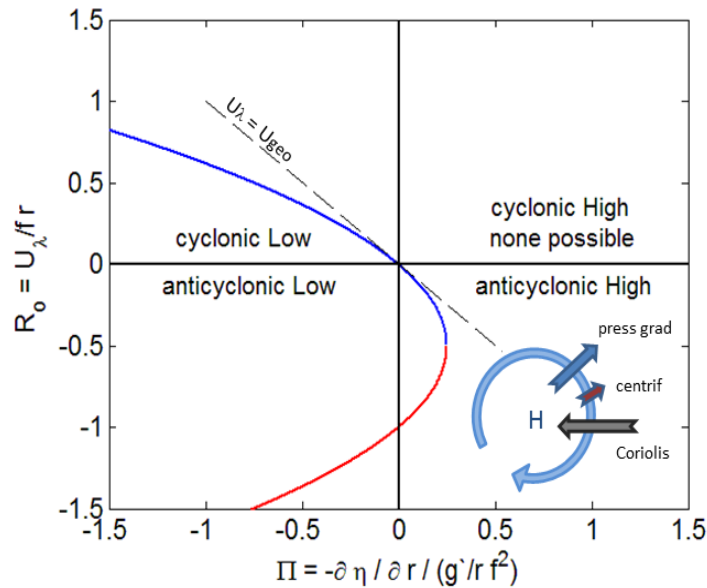


Figure 20: The blue and red line is the locus of possible solutions for gradient balanced flow over a large range of the nondimensional pressure gradient, Π . The blue line goes through the pure geostrophic case, $(\Pi, R_o) = (0, 0)$, and includes the most commonly observed eddies. Red denotes high anticyclonic solutions that are uncommon and often called anomalous, but not impossible insofar as gradient balance alone is concerned. The schematic force balance for a high anticyclone is in the appropriate quadrant. The high anticyclone of Fig. (18) has a very small Rossby number, about -0.03, so that the centrifugal force is much smaller than the Coriolis force and hence it falls on the blue curve, close to the origin and close to the line $U_\lambda = U_{geo}$.

1262 unimportant; the vortices that spill off the edges of a paddle or the vortex that forms in the convergent
 1263 flow above a drain are cyclostrophic eddies of this sort.

1264 The cyclonic and anticyclonic branches differ importantly in that the cyclonic branch goes through
 1265 the geostrophic state, $(0, 0)$, while the anticyclonic branch does not. This has implications for the
 1266 formation of such eddies. A cyclonic cyclostrophic eddy could result from the intensification (by vortex
 1267 stretching) of a larger scale, quasi-geostrophic flow whose absolute vorticity would be mainly planetary.
 1268 Tornadoes are most often cyclonic. On the other hand, an anticyclonic eddy is more likely to be formed
 1269 straightaway by intensification of whatever sign of relative vorticity might happen to be present at the
 1270 site of a convergence (vortex stretching) event. Dustdevils, small scale versions of tornadoes formed by
 1271 intense heating of the ground and subsequent convection, are about equally anticyclonic and cyclonic.

- 1272 3) While the allowable negative (low) Π has no upper limit, the maximum possible (high) Π is $1/4$
 1273 where $R_o = -1/2$. At that point the inward Coriolis force is balanced by the sum of outward pressure
 1274 gradient and centrifugal forces, which are equal. Still larger positive Π implies larger centrifugal force
 1275 which precludes a balance. This upper limit on Π has a real significance that can be seen in most
 1276 synoptic weather maps: high pressure centers are invariably regions with very low pressure gradient and
 1277 correspondingly low and often almost vanishing winds, i.e., high pressure centers give fair weather.
- 1278 4) The anticyclonic high regime has two possible solutions for $0 < \Pi < -1/4$, a small magnitude R_o
 1279 and a larger R_o solution ($R_o < 0$ in both cases). The former is predominantly geostrophic, with more or
 1280 less minor effect of curvature. This is by far the most commonly encountered anticyclone, and our
 1281 nominal oceanic eddy is of this sort. The larger magnitude R_o solution has stronger flow and the balance
 1282 includes a significant contribution from the centrifugal force. This is often referred to as an anomalous
 1283 anticyclonic high, on the basis that most winds or currents will generally be at least approximately
 1284 geostrophic (small R_o), and indeed, large R_o anticyclones are very seldom observed in nature.²¹
- 1285 5) An interesting case is anticyclonic flow at $(\Pi, R_o) = (0, -1)$ in which the balance is between the
 1286 outward centrifugal force and inward Coriolis force (vanishing pressure gradient). This is one of the
 1287 two kinds of inertial motion noted in Part 1, Sec. 5, vortical inertial motion, $U_\lambda = -fr$. Though possible
 1288 as a steady gradient balance, such a flow would be highly unstable (see footnote above), and unlikely to
 1289 persist in nature long enough to be observed.

1290 5.3 Problems

- 1291 (1) The discussion of curvature made allusion to centrifugal force acting on a parcel and is thus
 1292 inherently Lagrangian. Our shallow water model is Eulerian, and there must be an equivalent
 1293 representation of this process in the Cartesian form of the Eulerian momentum equations, Eqns. (14)
 1294 and (15). Can you discern what term(s) represent curvature? Hint: consider a control volume (in 2-d)
 1295 set on the northern edge of the eddy and estimate the net east-west advection of north-south momentum
 1296 into this control volume.
- 1297 (2) Using Fig. (20), show that the actual velocity of a balanced anticyclone having $\Pi \leq 1$ exceeds the
 1298 geostrophic velocity, and the reverse for cyclones. How about very intense, anticyclonic lows? What is

²¹This analysis considers only the possibility of a steady momentum balance, and on that basis an intense, high anticyclone is indeed possible. However, such eddies are rarely ever observed in nature. One contributing reason is that intense, high anticyclones tend to be vulnerable to centrifugal instability. Small perturbations in the azimuthally symmetric flow of an otherwise steady but unstable eddy may quickly escalate into chaotic flow that modifies the eddy away from its unstable configuration. Thus, even if an intense anticyclone was somehow formed, it would not survive. This goes beyond the present scope; see the excellent introduction by McWilliams (2006) and the review article by Chomaz, J. M, S. Ortiz, F. Gallaire and P. Billiant, 'Stability of quasi two-dimensional vortices', Lect. Notes Phys., **805**, 35-39 (2010), DOI 10.1007/978-3-642-11587-5_2

1299 the asymptote of R_o at very large positive Π ? Why is the other sign, $-\Pi$, completely different?

1300 (3) Sketch in the schematic force balance for the three quadrants of Fig. (20) not already noted.
1301 Describe the balance at $(\Pi, R_o) = (0, 0)$ and $(0, -1)$.

1302 (4) Fill in the algebra needed to go from Eqn. (75) to Eqn. (76), which is one possible way to
1303 nondimensionalize the solution for balanced flow, in effect, $R_o(\Pi)$. Show that another equally efficient
1304 form is U_λ/U_{geo} is some function of Π .

1305 6 Closing remarks

1306 6.1 Summary

1307 In Section 1 we asked, **What circumstances lead to a near geostrophic balance?** To develop some
1308 insight we analyzed several experiments on geostrophic adjustment posed in a numerical, shallow water
1309 model. The experiments started with a thickness anomaly having a horizontal scale $L = 100$ km and
1310 amplitude, $\eta_0 = 50$ m, comparable to observed mesoscale eddies. Once released, the anomaly was free
1311 to evolve according to the physical processes allowed.

1312 **1) When rotation is omitted by setting $f = 0$, the anomaly is quickly and completely dispersed in**
1313 **space by the propagation of shallow water gravity waves.** These waves are nondispersive, having
1314 phase speed and group speed $C = \sqrt{gH} \approx 3$ m sec⁻¹ for the stratification typical of the mid-latitude
1315 oceans. These gravity waves are the only possible nontrivial free motions when $f = 0$. In the
1316 one-dimensional, gravitational adjustment problem of Sec. 3, the solution consists of discrete,
1317 propagating pulses that retain the shape of the initial ridge and so look nothing like elementary (sine)
1318 waves.

1319 A given experiment is characterized also by the amplitude of the initial thickness anomaly, η_0/H .
1320 If the initial amplitude is small, $\eta_0/H \ll 1$, the pulses propagate at very nearly the expected gravity
1321 wave speed, C . For a larger initial amplitude, say $\eta_0/H \geq 0.2$, finite amplitude effects include
1322 distortions (from linear) in the shape of the pulses, and a systematic change in the propagation speed
1323 depending upon the sign of η_0 .

1324 **2) When rotation is included by an f -plane approximation, the transient response includes gravity**
1325 **waves that are more or less modified by rotation, and a possible steady state.** The wave frequency
1326 depends upon wavelength compared to the radius of deformation, $R_d = C/f$, the intrinsic horizontal
1327 length scale of a rotating, shallow water system. The highest frequency and shortest waves are

1328 nondispersive gravity waves, while longer wavelengths are near-inertial rotary motions having very
 1329 large phase speed but very small group speed. Aside from the short wave high frequency limit,
 1330 inertia-gravity waves are highly dispersive and so the radiating waves do not retain the structure of the
 1331 initial thickness anomaly.

1332 **3) If the initial ridge is a potential vorticity anomaly with respect to the outlying fluid, and if the**
 1333 **initial ridge is sufficiently wide compared to R_d , then some fraction of the ridge will survive the**
 1334 **adjustment process and reach geostrophic balance.** In the case of a one-dimensional ridge, the
 1335 geostrophic current takes the form of jets whose half-width is R_d . In an inviscid f -plane experiment,
 1336 geostrophic balance can be exact, and exactly steady, i.e., could persist forever. (As we will see in Part
 1337 3, this is not the case when the latitudinal variation of f is also considered.) In a two-dimensional
 1338 experiment, an exactly steady balance is also possible, and may include a flow curvature effect
 1339 proportional to the Rossby number, U/fL , with U the current speed.

1340 If a calculation of the final, geostrophically balanced state of an essentially linear experiment had
 1341 been the only goal, then the best route would surely be the analytic solution of Section 4.4 built upon q
 1342 conservation and geostrophy. On the other hand, if the need was to know the inertia-gravity waves that
 1343 accompany geostrophic adjustment or if the experiment was in a large amplitude regime, then it would
 1344 be necessary to solve the full shallow water momentum and continuity equations that contain
 1345 q -conservation plus gravity wave dynamics and nonlinear processes.

1346 This concludes our discussion of the classical (f -plane) geostrophic adjustment problem, and it is
 1347 fair to ask if we can now claim to understand the circumstances that lead to a near geostrophic balance
 1348 of ocean gyres and mesoscale eddies. The rotating, shallow water geostrophic adjustment experiments
 1349 of Secs. 4 and 5 lead us to expect that a mass and potential vorticity anomaly having the width,
 1350 stratification and rotation of a mid-latitude oceanic mesoscale eddy should adjust spontaneously to a
 1351 near geostrophic balance given the absence of strong bottom friction or other external force. This
 1352 positive result is not sensitive to numerical or physical details.²² To understand geostrophic balance in
 1353 the fullest sense requires knowing the limits in parameter space (at what L/R_d , η_o/H etc.) this result
 1354 will *not* hold, and to know at least a little of what happens then. This is going to require some further
 1355 experimentation and analysis. Running a new experiment is as easy as changing one of the parameters
 1356 of the physical problem, e.g., the latitude or the initial ridge width. To gain some confidence in the
 1357 numerical solution one might experiment with some details of the numerical model as well, e.g., the
 1358 grid interval, time step, etc. With some experience it will become evident that the subsequent cataloging
 1359 and interpretation of the result is best couched in terms of one of the derived parameters — the radius of
 1360 deformation and the potential vorticity — which offer a very significant economy. To this point then, it

²²This leaves open why there are mass anomalies in the first place. This is a very important question that goes well beyond the present discussion, but, see e.g., Tulloch, R., J. Marshall, C. Hill and K. S. Smith, 'Scales, growth rates and spectral fluxes of baroclinic instability in the oceans', *J. Phys. Oceanogr.*, **41**, pp 1057-1076, 2011. DOI: 10.1175/2011JPO4404.1.

1361 appears that we have a solvable and relevant model of geostrophic adjustment, and a few key concepts
1362 that will help interpret new model solutions and so help us develop greater intuition for geostrophic
1363 balance.

1364 6.2 What comes next?

1365 An understanding of geostrophy is an essential first or second step in a study of the atmosphere and
1366 ocean, but be assured that there is much, much more to learn about how such geostrophic features come
1367 to exist in the first place, and how they evolve. In Part 3 we will take up a fundamental question that
1368 comes from a second look at the large scale mass (pressure) and circulation fields of the ocean and
1369 atmosphere, *viz.*, **How do small departures from geostrophic balance lead to time-dependence and**
1370 **to the marked east-west asymmetry of low frequency phenomenon?** The plan is again to solve
1371 experiments in geostrophic adjustment, the next time taking account of the very important latitudinal
1372 variation of f .

1373 6.3 Supplementary material

1374 The most up-to-date version of this essay plus the Matlab and Fortran source codes noted in the text
1375 may be downloaded from the author's public access web site:

1376 www.whoi.edu/jpweb/aCt.update.zip

1377 Matlab and Fortran source codes include the following, all of which are public domain for all
1378 educational purposes.

1379 **twowaves.m** shows the result of superposing two sine waves whose dispersion relation may be
1380 specified arbitrarily.

1381 **twolayer_eig.m** solves for eigenmodes of two and three layer models using symbolic math.

1382 **ftransform.m** solves an initial value problem in one-dimension and without rotation. Shows the wave
1383 forms that result from dispersion that is normal, anomalous or none.

1384 **geoadj_1d.m** is a shallow water model used for the one-dimensional geostrophic adjustment
1385 experiments of Secs. 3.1 and 3.2. The latitude, thickness anomaly, friction, etc. may be easily varied
1386 from experiment to experiment. These all assume that the initial velocity vanishes.

1387 **geoadj_1d_uic.m** as above, but in this script the initial condition includes several choices for the initial
1388 current, including vanishing potential vorticity.

1389 **geoadj_2d.for** is a two-dimensional shallow water model used to do the geostrophic adjustment
1390 experiment of Sec. 5. Written in a very simple Fortran. Solutions like those shown in Sec. 5 can be
1391 generated on a reasonably capable PC in a few minutes. Model parameters including latitude, the kind
1392 of f model, eddy amplitude, etc. are entered from the keyboard. Output is saved to disk.

1393 **galook.m** is a Matlab script used to plot the data generated and saved by **geoadj_2d.for**.

1394 The additional animations are:

1395 **ga2d_eta_latxx.mpg**; animations of thickness anomaly, η , for latitude $xx = 10, 20, 40,$ and 60°N .

1396 **ga2d_u_latxx.mpg**; the currents that go with the η animations above.

Index

- 1397 barotropic
- 1398 phase speed, 29

- 1399 a priori, 40

- 1400 baroclinic, 25
- 1401 baroclinic mode, 30
- 1402 barotropic
- 1403 mode, 27
- 1404 Burger number, 46

- 1405 curvature, 56

- 1406 d'Alembert solution, 36
- 1407 dispersion relation, 15
- 1408 inertia-gravity waves, 42

- 1409 energy balance, 16, 48
- 1410 Eulerian velocity field, 15

- 1411 f-plane, 42
- 1412 floats, 16
- 1413 flux form, 10
- 1414 Froude number, 40

- 1415 geostrophic motion, 48
- 1416 gravitational adjustment, 34

- 1417 hydrostatic pressure, 11

- 1418 ideal fluid, 8
- 1419 inertial motion
- 1420 inertial oscillation, 47
- 1421 vortial inertial motion, 60

- 1422 Lagrangian velocity, 16
- 1423 longitudinal relationship, 37

- 1424 mass conservation, 10
- 1425 mass or thickness balance, 10
- 1426 material derivative, 10

- 1427 momentum flux, 11

- 1428 nondispersive, 36
- 1429 normal mode, 26

- 1430 passive tracer, 15
- 1431 polarization, 44
- 1432 potential vorticity, 17
- 1433 and gravity waves, 39
- 1434 potential vorticity conservation, 49
- 1435 potential vorticity conservation equation, 20

- 1436 radius of deformation, 45
- 1437 reduced gravity approximation
- 1438 justification, 31
- 1439 Rossby number, 57
- 1440 rotation time, 45

- 1441 shallow water criterion, 8
- 1442 shallow water equations, 12
- 1443 shallow water model, 7

- 1444 transverse relationship, 37

- 1445 vorticity, 18
- 1446 absolute vorticity, 20
- 1447 planetary vorticity, 20
- 1448 relative vorticity, 20
- 1449 vorticity field, 18

- 1450 wave group speed, 15
- 1451 wave phase speed, 15